81-10-07

MEASUREMENT OF 1-30 MEV CELESTIAL GAMMA RAYS WITH AN IMAGING COMPTON TELESCOPE

'COMPTEL'

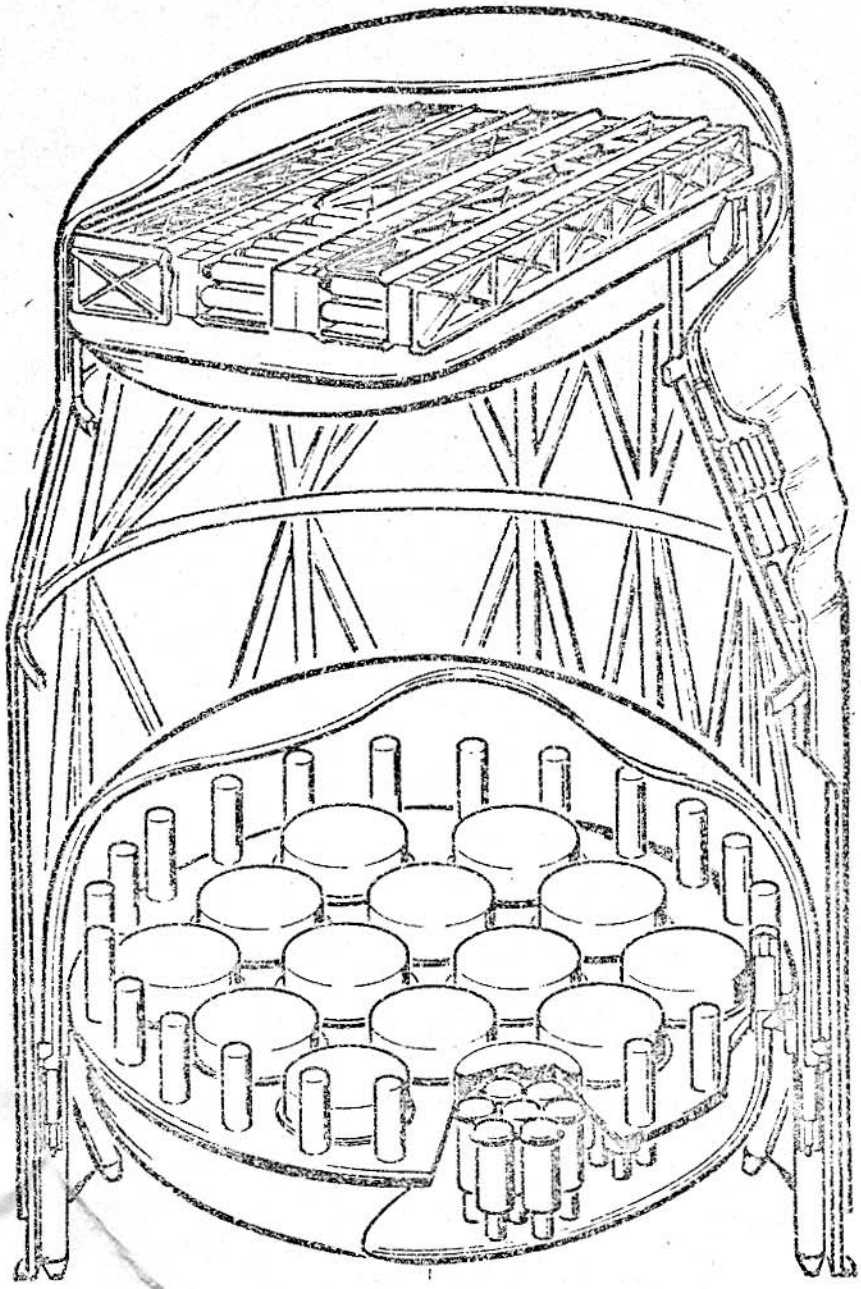

PROPOSAL FOR A GRO-EXPERIMENT

INVESTIGATION AND TECHNICAL PLAN

MAX-PLANCK-INSTITUT
FÜR EXTRATERRESTRISCHE PHYSIK, GARCHING
COSMIC RAY WORKING GROUP, UNIVERSITY OF LEIDEN
SPACE SCIENCE CENTER, UNIVERSITY OF NEW HAMPSHIRE
SPACE SCIENCE DEPARTMENT OF ESA

1978

Measurement of 1-30 MeV Celestial Gamma Rays with an Imaging Compton Telescope "Comptel".

Proposal for a GRO-Experiment

Investigation and Technical Plan

Principal Investigator
V. Schönfelder
Physicist, High Energy Astrophysics
49-89-3299578 (Munich)
Max-Planck-Institut
für extraterrestrische Physik
D-8046 Garching
Germany

Co-Principal Investigators
B.N. Swanenburg
Head of Cosmic Ray Group
071-148333 Ext. 5817
Cosmic Ray Working Group
University of Leiden
Leiden, The Netherlands

J.A. Lockwood
Prof. of Physics
(603) 862-2000
Department of Physics
University of New Hampshire
Durham, New Hampshire 03824

B.G. Taylor
Head of High Energy Astrophysics
Division
1719-8-2590
Space Science Department of ESA
ESTEC
Noordwijk, The Netherlands

Co-Investigators
G. Kanbach
Physicist, High Energy Astrophysics
49-89-3299851
Max-Planck-Institut
für extraterrestrische Physik
D-8046 Garching
Germany

F. Melzner
Head of Engineer Section
49-89-3299517
Max-Planck-Institut
für extraterrestrische Physik
D-8046 Garching
Germany

J.A.M. Bleeker
Physicist, High Energy Astrophysics
071-148333 Ext. 5817
Cosmic Ray Working Group
University of Leiden
Leiden, The Netherlands

A.J.M. Deerenberg
Physicist, High Energy Astrophysics
071-148333 Ext. 5817
Cosmic Ray Working Group
University of Leiden
Leiden, The Netherlands

W. Hermsen
Physicist, High Energy Astrophysics
071-148333 Ext. 5817
Cosmic Ray Working Group
University of Leiden
Leiden, The Netherlands

W.R. Webber
Prof. of Physics
603-862-2756
Department of Physics
University of New Hampshire
Durham, New Hampshire 03824

K. Bennett
Physicist, High Energy Astrophysics
1719-8-2203
Space Science Department of ESA
ESTEC
Noordwijk, The Netherlands

R.D. Wills
Physicist, High Energy Astrophysics
1719-8-2591
Space Science Department of ESA
ESTEC
Noordwijk, The Netherlands

February 3, 1978

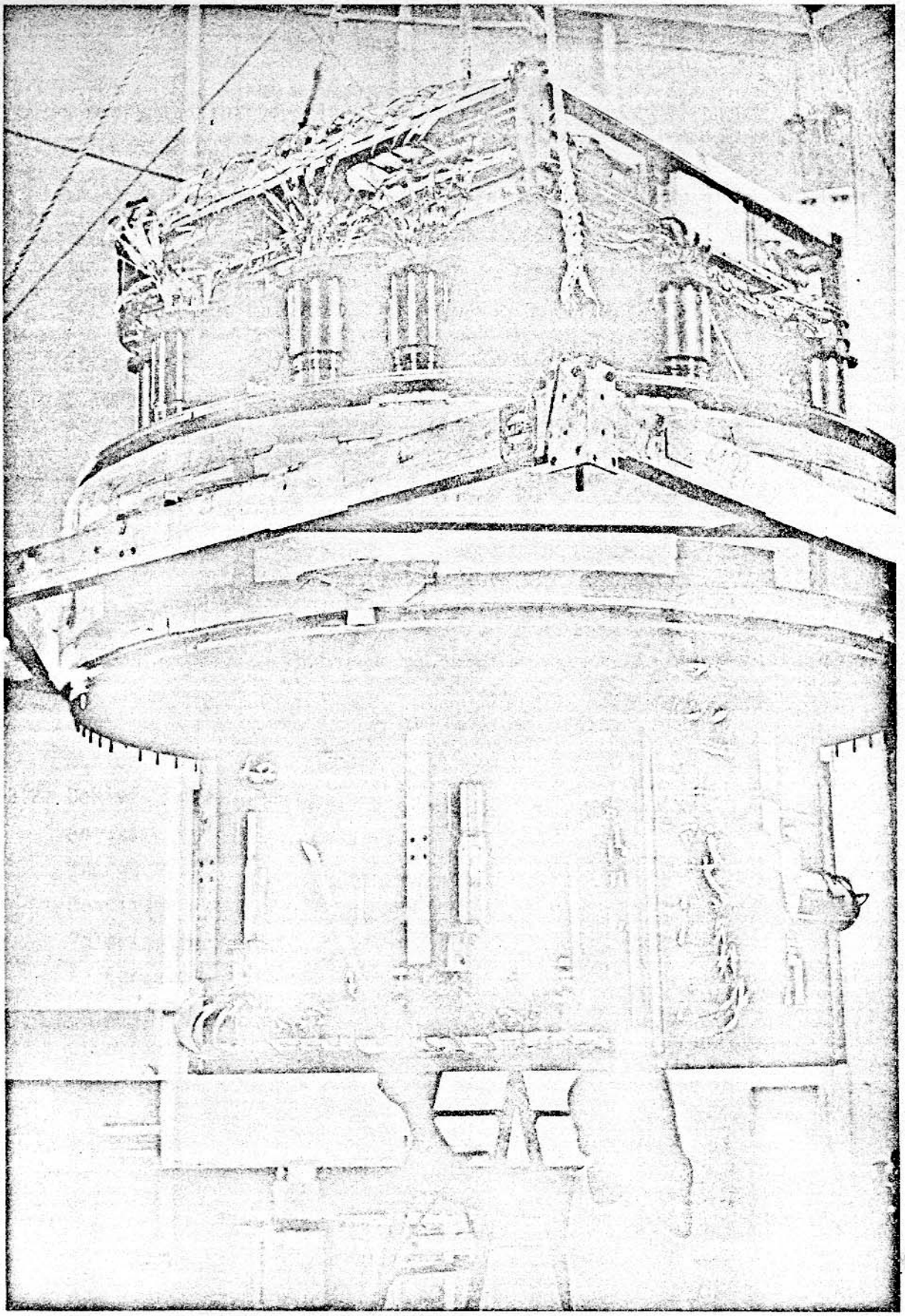

The new Compton Telescope of the Max-Planck-Institut some days before its first balloon flight in October 1977.

TABLE OF CONTENTS

		Page
	Summary and Introduction	1
1.	Scientific Objectives	2
1.1	Point Sources	2
1.2	Diffuse Emission from the Galaxy	3
1.3	Cosmic Diffuse Flux	5
1.4	Broadened Line Emission	6
	Other Objectives	7
2.	Experiment Description	8
2.1	Concept of Investigation	8
2.2	Description of the Telescope	9
2.3	Electronics	10
2.4	Mechanical Design	11
3.	Instrument Performance	13
3.1	Requirements and Detector Performance	13
	Time-of-flight measurement	13
	Pulse-shape measurement	13
	Location of the scattering process	14
	Energy resolution of the scintillation detector	14
	Anticoincidence shield	15
3.2	Derived Properties of the Telescope	15
	Angular resolution	15
	Energy resolution	17
	Sensitive area	17
	Polarization	18
	Background radiation	18
3.3	Detection Sensitivity and Expected Results	21
4.	Observation Programme	21
5.	Calibration and Data Analysis	23
6.	Management Summary	24
7.	Conclusions	25
	Appendices	26
A.1	Sensitivity Calculations	26
A.2	References	29

Summary and Introduction

Experience at all wavelengths in astronomy has shown that with a carefully designed low background instrument, the scientific return is always high when exploring a new energy domain and there are many surprises in the data acquired. Recent examples of this are the SAS-2 and COS-B high energy gamma ray instruments which have discovered gamma ray pulsars (Fichtel et al., 1975) as well as a new class of gamma ray objects (Hermsen et al., 1977).

Previous investigations in the 1-30 MeV gamma ray region have been motivated by the knowledge that unique astrophysical phenomena may become observable in this range between X-ray energies and high energy gamma rays. Many attempts have been made to measure the flux and spatial distribution of these intermediate energy photons using balloon and satellite-borne instrumentation. However, the results obtained to date have largely been conflicting and unconvincing compared with the high quality measurements made at energies above and below this range.

The basic difficulty is one of instrumental background which is present in all shielded and unshielded single element detectors and even in earlier versions of the Compton telescope. Suppression of this instrumental background to an acceptable level is therefore the key to successful measurements in this energy range.

This proposal demonstrates how the concept of an imaging Compton telescope, brought to the state of the art level, can overcome these background difficulties and provide unprecedented sensitivity and spatial resolution in this energy range. The strength of the imaging Compton telescope arises from the following:

1. A coincidence between two detectors is required to register the passage of a gamma ray.
2. A genuine gamma ray event is further validated by measuring the time of flight of the gamma ray between the two detector arrays.
3. Pulse shape discrimination in the upper detector arrays is used to separate gamma rays from neutrons.

   These three requirements reduce the instrumental background to a level well below that of the diffuse cosmic background flux.
4. The powerful imaging properties of the telescope provide a combination of a wide field of view, high spatial resolution and simultaneous gamma ray source and background (mainly diffuse cosmic) measurement.
   The low instrumental background combined with the imaging properties results in detection limits which are determined by counting statistics only.
5. The telescope provides an energy resolution commensurate with many interesting predicted spectral features.
   The proposed telescope is a logical extension of previous balloon-borne telescopes. The parameters of the proposed system are based on experience gained in this balloon program, recent laboratory tests, and calculations based on known cross sections for electromagnetic interactions. A summary of these parameters is given in Table I.

Energy range:	1-30 MeV
Sensitive area:	20-50 cm^2
Angular resolution:	2.0^o- 6.0^o(FWHM)
Energy resolution:	$\approx$ 10% FWHM
Geometrical factor:	5-30 cm^2 ster
Field of view:	$\approx$ 1 ster
Minimum source detectability at 5 σ above 1 MeV (1 month):	$5 \cdot 10^{-5}/cm^2 s$ (= 2% of the expected total Crab emission)

This telescope flown on GRO will, for the first time, bridge the gap between X-ray and high energy gamma ray astronomy and offers a unique opportunity to open a new era of extragalactic gamma ray astronomy.

1. Scientific Objectives

The energy domain from 1-30 MeV gamma rays is one of the least well understood parts of the electromagnetic spectrum. Definitive observations in this energy range will help to interpret a range of astrophysical problems from those of compact stellar objects to the universe as a whole. In this energy range the gamma ray production mechanisms undergo a transition from low energy processes such as thermal emission to a variety of high energy processes like inverse Compton radiation, π^0-radiation, nuclear radiation, etc. Studies in this transition energy range will therefore provide sensitive tests and constraints on the various production mechanisms.

The imaging character, the broad effective aperture and low background characteristics of the imaging Compton telescope we propose dictate the principal scientific objectives. These can be broadly grouped under the following headings:

1) Study of Point Sources
2) Study of Diffuse Emission from the Galaxy itself
3) Study of the Cosmic Diffuse Flux
4) Study of Broadened Line Emission.

We will now treat each of these areas separately.

1.1 Point Sources

A summary of the intensities of a variety of point sources over a wide range of energies is given in Figure 1. These data are presented in a form in which the inten-

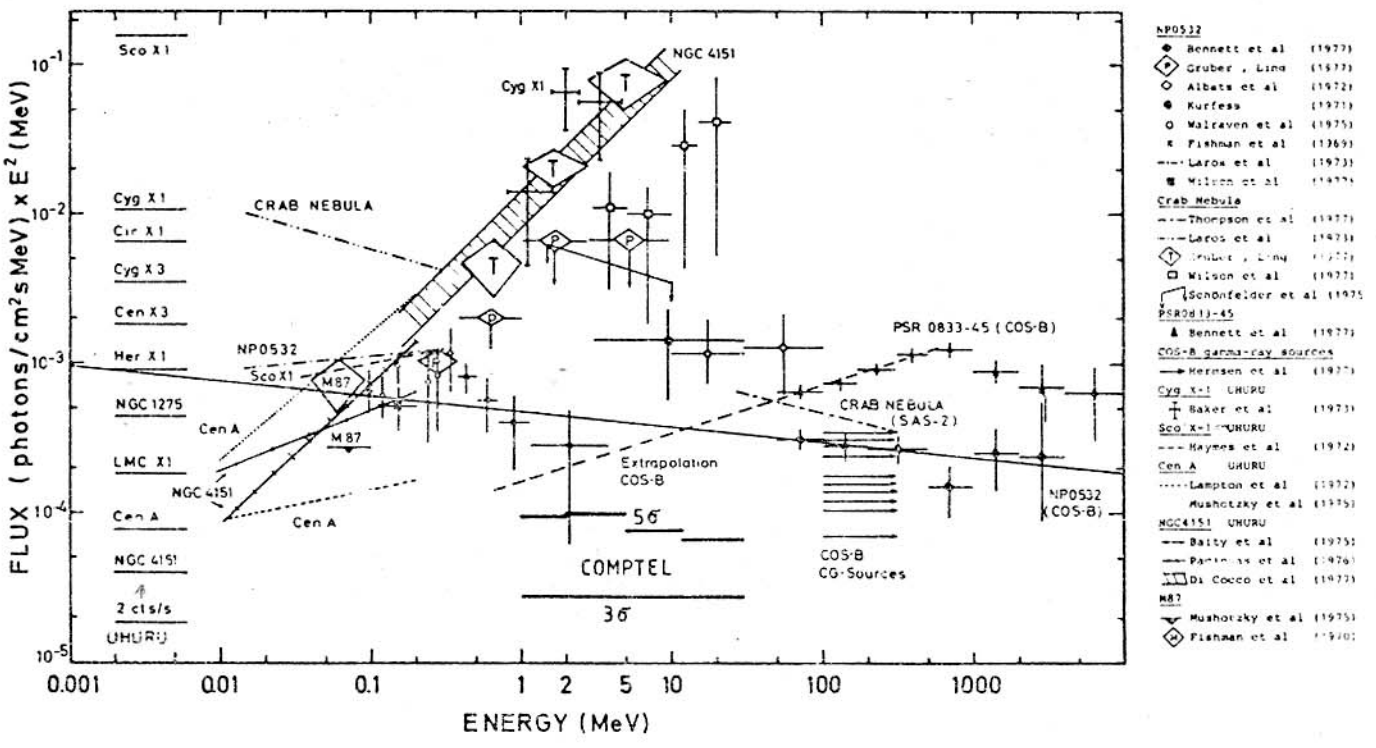

Fig. 1: Summary of data on spectra of point sources. Intensities are multiplied by E^2.

sities are multiplied by E^2, a procedure which illustrates more clearly spectral features and relative intensities. Also included in this figure are the sensitivity limits of our experiment as calculated later in this proposal. Several aspects of the current data are of interest. First, several gamma ray sources have recently been observed by

COS-B and SAS-2. These sources have no X-ray or optical counterparts. Second, there are a large number of X-ray sources which have no gamma ray counterpart ever though in many cases one might be expected from a simple extension of the spectra. This is particularly true for several extragalactic sources. Clearly, measurements between 1-30 MeV at our expected sensitivity levels will provide an understanding of the spectral behaviour of most of these sources and thereby assist greatly in the interpretation of the radiation processes as well as the parameters pertinent to each mechanism.

Our typical sensitivity level is $\sim 1/50$ of the expected intensity of the Crab nebula so that the confused observational situation that exists at intermediate energies will easily be resolved.

Extrapolation of spectral data from X-ray energies indicates that there are several regions of the galactic plane where, at our level of sensitivity, source confusion will become important unless the angular resolution of the telescope is $\sim 3^0$ or better. Our telescope meets this goal which is also comparable with the expected resolution for instruments surveying the higher energy part of the spectrum above 30 MeV.

With its large effective aperture and good spatial resolution the imaging Compton telescope is especially suitable for the simultaneous study of the temporal variations of many point sources. Here again the emission mechanisms responsible for these variations may well be different at high and low energies with the intermediate energy range representing a transition region. Correlations of the temporal behaviour we observe at intermediate energies with that observed at higher and lower energies will be very useful for understanding the processes responsible for these variations.

1.2 Diffuse Emission from the Galaxy

The features of the galactic plane diffuse emission emerge more clearly as one goes to higher energies. For example, the galactic disk is barely visible at X-ray energies but emerges clearly at energies ~ 100 MeV according to the observations of SAS-2 and COS-B. Many authors have considered the origin of this diffuse flux. As an example, Figure 2 shows the computed differential gamma ray production rates for various mechanisms in the local galactic environment. Here again there is a transition from the π^0 source mechanism which is prominent above ~ 100 MeV to the bremsstrahlung and inverse Compton processes which become more important at lower energies. Each process gives different information on the matter, magnetic field and cosmic ray distribution in the galaxy. Accurate spectral measurements of this emission, clearly free from instrumental background effects, will be crucial to the separation and evaluation of the various components. As an example of the current uncertain situation regarding the gamma ray spectrum in this intermediate energy range, we show in Figure 3 a summary of measurements in the direction of the galactic center. Again the data are presented in a form in which the intensities are multiplied by E^2 and the expected sensitivity limits of our experiment are shown. It is once again clear that background free measurements at this level of sensitivity will finally enable the full interpretative power of gamma ray astronomy to be utilized directly for the study of galactic structure and properties.

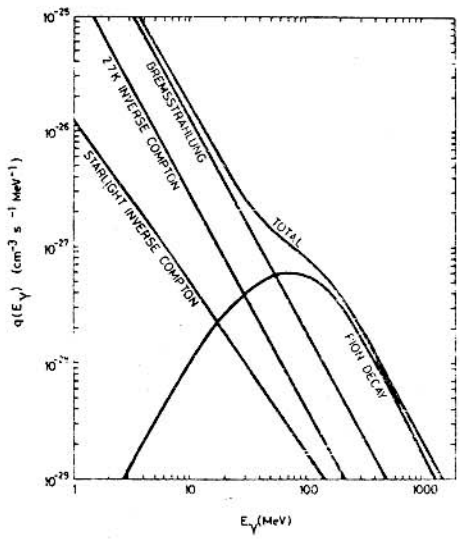

Fig. 2: Local gamma ray production rates from various emission mechanisms

Another important aspect of this problem concerns the spatial structure of the galactic disk emission. SAS-2 and COS-B have made important contributions to this aspect of the problem because of their relatively

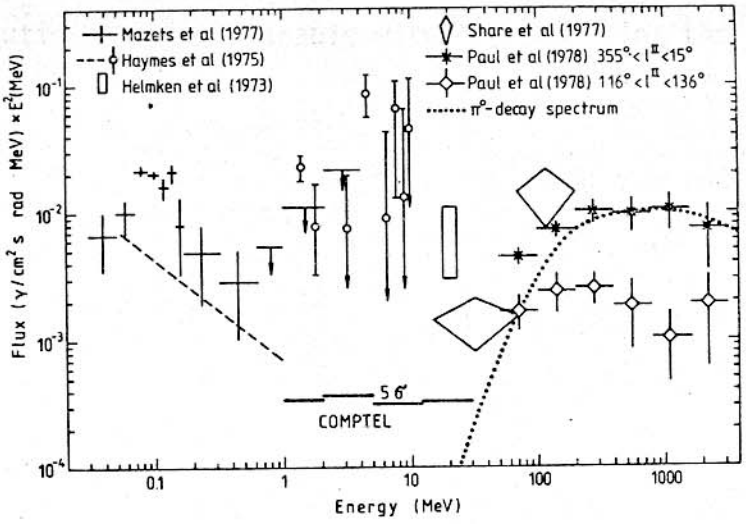

Fig. 3: Summary of data on the spectrum of galactic diffuse emission at longitudes near the galactic center. Intensities are multiplied by E^2.

good angular resolutions which are $\sim 3^0$. From these data we show an estimate of the galactic gamma ray distribution with latitude for several energies at a longitude $l^{II} = 335^0$ in Figure 4. This figure uses data on the latitude distribution of gamma ray emission > 100 MeV from Fichtel et al. (1976), the estimate of the cosmic background emission in Figure 5 of this proposal and assumes that the shape of the latitude distribution does not change from 1 to 100 MeV. Several features of this figure are of interest. The first relates to the enhancement of the disk relative to the cosmic diffuse emission. At high energies this enhancement is large (~30:1) and easily observable whereas at 1 MeV this enhancement is only ~ 2:1 and at 10 MeV ~ 3:1. This means that to adequately study the spatial properties of this emission in the 1-30 MeV region requires an angular resolution at least as good as that obtained in the SAS-2 experiment coupled with an instrumental background which is less than the cosmic diffuse background. In the anti-center direction the enhancement of the disk emission relative to the diffuse emission is even less, requiring much more stringent limits on the angular resolution and instrumental background to extract useful data. As discussed later in this proposal, our estimated angular resolution is typically 3^0 FWHM and our background level generally will be much less than the cosmic diffuse flux.

The second aspect of Figure 4 relates to the details of the latitude structure of the disk itself. The latitude distribution may change as one goes from higher to lower energies because the relative importance of different emission mechanisms may change. Local "hot-spots" arising from cloud structure or a particular distribution of sources may be present. The ability to detect and interpret these details will be commensurate with the angular resolution capabilities of the telescope. Our telescope design is motivated by a requirement to observe these expected details along with a practical reso-

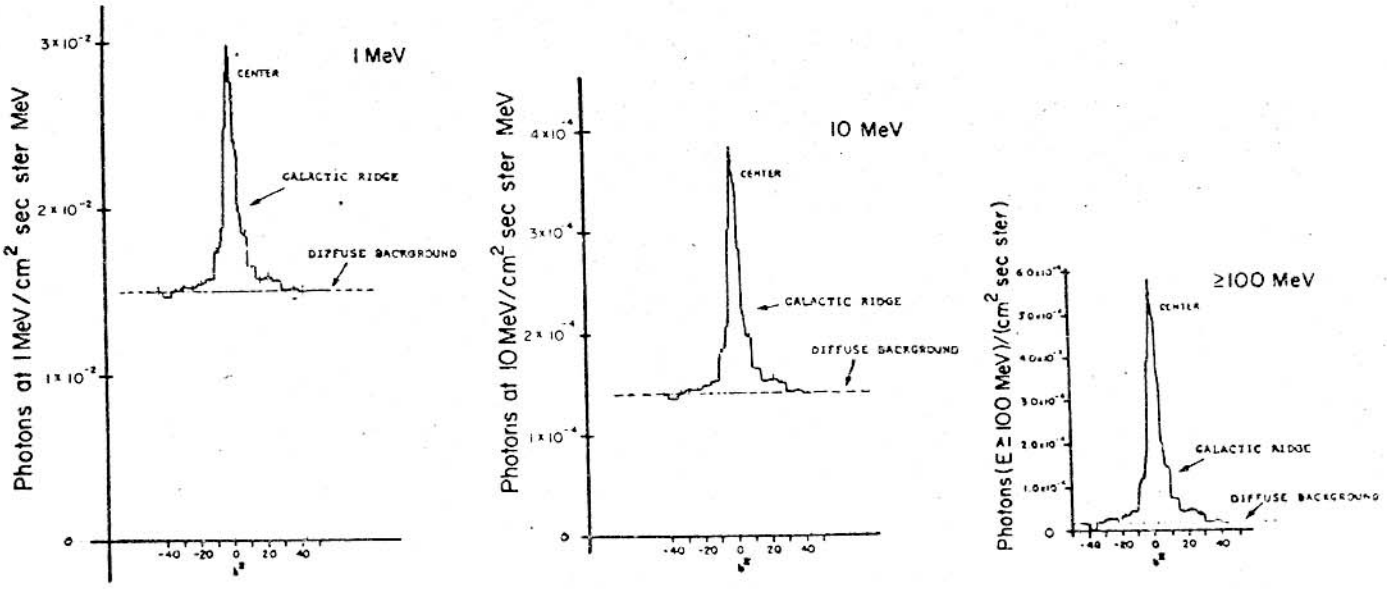

Fig. 4: Gamma ray distribution as a function of latitude for energies of 1, 10 and 100 MeV centered on $l^{II} = 335^0$.

lution limit comparable with objectives of the high energy gamma ray experiments expected to be on GRO.

1.3 Cosmic Diffuse Flux

In the X-ray and high energy gamma ray regions of the spectrum a diffuse flux is observed at high galactic latitudes. Experimentally and theoretically this situation has been widely discussed in the literature and interpreted in terms of a cosmic diffuse flux. A recent compilation of this cosmic diffuse flux is shown in Figure 5. It is clear from this figure that there is a large uncertainty in the data in the 1-30 MeV range, while at the same time the possibility of a significant spectral feature exists. Spectral measurements in this energy interval are therefore of extreme importance for interpreting the origin of this radiation.

In addition to energy spectral easurements, anisotropy or "clumpiness" measurements will be crucial to the understanding of the origin of this diffuse flux. A significant fraction of this diffuse radiation may come from a number of undetected superimposed localized sources - e.g. clusters of galaxies. Depending on the production mechanisms, diffuse emission in this energy range may originate in fewer and more intense sources than for the X-ray domain. Hence one might expect changes in the clumpiness as a function of energy. Again the imaging Compton telescope with its large aperture and good angular resolution is very well suited for granularity-anisotropy studies of this radiation.

Observations of the cosmic diffuse flux will obviously be limited by local background production in the telescope and its environment. Our imaging Compton telescope has a unique ability to achieve low background levels if all of the subtleties of the technique are fully exploited.

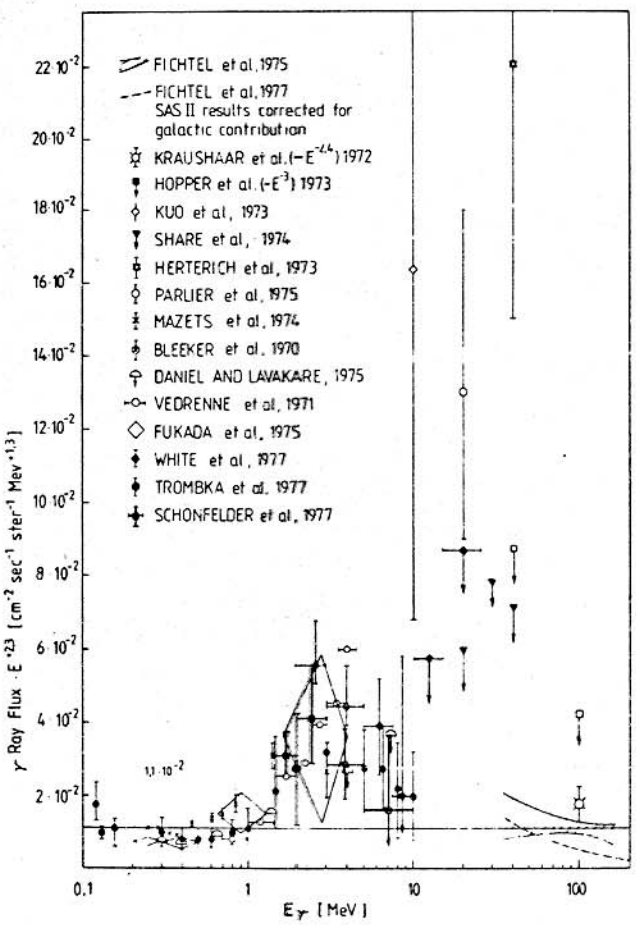

Fig. 5: Summary of data on the spectrum of the cosmic diffuse flux. Intensities are multiplied by $E^{2.3}$.

In addition, the data itself may be used to understand the origin of the remaining instrumental background and to correct for it. The problem of the instrumental background and the limits we expect to achieve for our telescope are discussed elsewhere in this proposal. The basic background and some of its components are shown in Figure 6 along with the diffuse flux. After correction the eventual background will be in the range 10-30% of the expected cosmic diffuse flux. An instrumental background at this level will allow significant measurements of the energy spectrum and spatial distribution of the high latitude cosmic duffuse flux.

1.4 Broadened Line Emission

Gamma ray lines from excited nuclei are of great astrophysical significance. Many of these lines may be broadened by various processes and in these cases the superior resolution of cooled solid state detectors cannot be fully utilized. The fact that our telescope contains nearly 1 m^2 NaI detectors with a 10% energy resolution dictates that a study of possible broadened line emission, utilizing these detectors, be a primary scientific objective of our studies. In Figures 7A and B we summarize some current measurements and predictions for gamma ray lines from localized sources and diffuse sources along with the predicted sensitivity limits for our telescope. Suffice it to say that these limits are considerably lower than any of the currently reported gamma ray line intensities and better than proposed limits from many specialized gamma ray line experiments! This is the case for both localized gamma ray sources and extended sources, such as the interstellar medium. In this latter case, gamma ray line observations can be expected to provide information on the interstellar abundance of C and O atoms for example and the intensity of 10 MeV/nuc cosmic rays. These lines will have a broad component arising from cosmic ray C or O and a narrow component resulting from interstellar C or O excited by cosmic rays. Spatial variations of any line emission of this nature can be directly interpreted in terms of the galactic distribution of the parent nuclei.

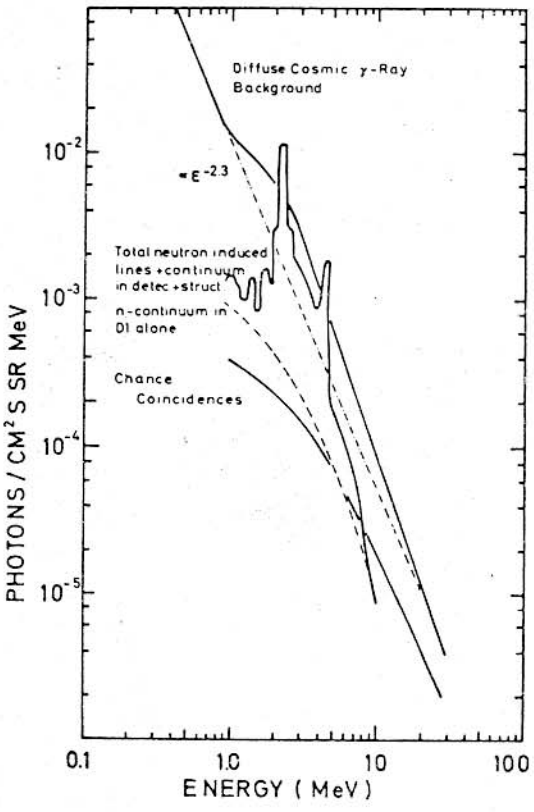

Fig. 6: Calculated expected instrumental background together with the observed cosmic gamma ray diffuse background.

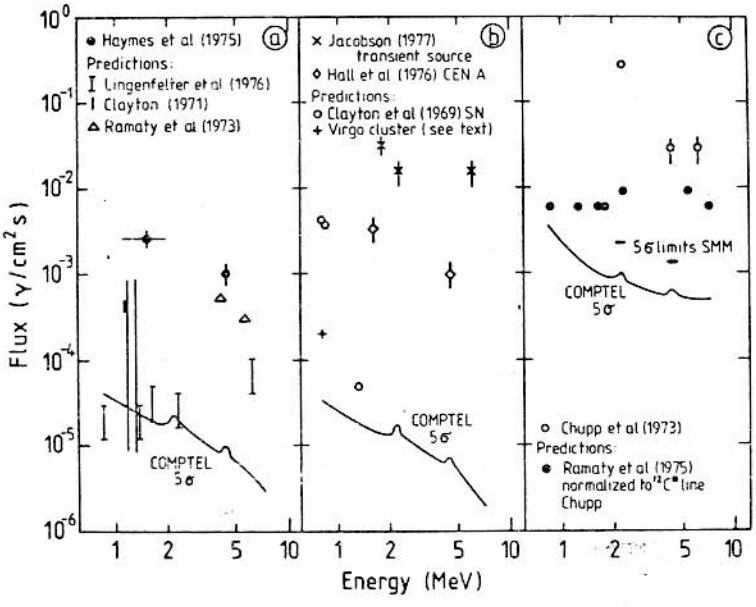

Fig. 7: Measured and predicted gamma ray line intensities and our predicted sensitivity limits.
A) diffuse galactic, B) point sources, C) solar flares.

Lingenfelter and Ramaty (1976) have made estimates of the relative intensities of gamma ray lines resulting from this process. The absolute intensities are dependent on many uncertain parameters. If we normalize these intensities to the 4.4 MeV line intensity "observed" by Haymes et al. (1975) in the direction of the galactic center we have the expected intensities for several lines as indicated in Figure 7A. Most of these lines would be observable with our instrument. If the 4.4 MeV line is lower than observed by Haymes et al., but compatible with the calculations of Ramaty and Lingenfelter (e.g. $\sim$ 3-6 x 10^{-4} photons/cm^2 sec in the direction of the galactic center) then this line would still be easily observable by our telescope although several of the weaker ones would not.

With regard to true point sources of line emission several possible observations and some predictions are shown in Figure 7B. We note that gamma ray line intensities have been estimated for explosive nucleosynthesis in supernova events (Clayton and Fowler, 1969). These relatively optimistic estimates, indicated in Figure 7B, give fluxes of key gamma ray lines of $> 10^{-3}$ photons/cm^2 sec at a distance of 1 Mpc lasting for several days. For example, observing the Virgo cluster of galaxies at a distance of 15 Mpc and integrating over the entire 12^o of the cluster, therefore integrating in time over $\sim$ 50 SN per year, would lead to fluxes of the Ni line (0.81 MeV) $\sim 2 \times 10^{-4}$ photons/cm^2 sec - easily observable with our instrument.

At least one solar gamma ray line (2.2 MeV) has definitely been observed in a solar flare at a level of 2.8×10^{-1} photons/cm^2 sec (Chupp et al., 1973). Several lines should be expected from nuclear interactions produced by solar cosmic ray protons. The intensity of these lines is correlated in time with the intensity of the energetic particles in the flare region. A study of the temporal variation of different lines allows a detailed investigation of the flare process and the environment of the solar atmosphere. Line emission from the sun and other flare type stars will be in sought by our telescope.

These measurements can be carried out in both the double Compton and single element NaI crystal mode. The best sensitivities are in the double Compton mode if the sun is in the field of view. Then they are typically a factor ~ 2 better than those achievable in a specially designed experiment for solar gamma rays on the SMM (See Figure 7)! One would therefore expect correspondingly valuable and interesting results.

The single element NaI crystal mode has the advantage of a nearly 2π viewing aperture and the sensitivities in this mode are still comparable to those exptected on the SMM.

Other Objectives. The combination of the various elements in the Compton telescope provides a very effective gamma ray burst detector. We are including a burst mode in the data handling electronics. The most sensitive burst indicator is the top bank of scintillators which will be used to trigger on bursts of size $\geq 3 \times 10^{-7}$ erg/cm^2 with E $\geq$ 50 keV. The energy spectrum and temporal history of the burst will then be determined using data from the lower NaI scintillators.

Finally, it may be pointed out that the Compton telescope provides the possibility of detecting linear polarization from gamma ray sources. Polarized gamma rays may originate under extreme conditions due to the influence of strong magnetic fields although predictions of observable intensities have not been published. Detection of such polarization would provide a vital clue to the emission mechanism of such an exotic object.

2. Experiment Description

2.1 Concept of Investigation

The Compton telescope may be considered as the extension of the optical imaging technique to gamma ray energies. In case of the optical camera the photon is first scattered in the lens and then detected by a second interaction on the film. The geometrical representation of an astronomical observation with a Compton telescope is shown in Figure 8. The infalling gamma ray of energy E_γ is Compton scattered in a first interaction and the scattered gamma ray E_γ' is absorbed in a second interaction process. By measuring the energy losses E_e' and E_e'' in both interactions and by measuring the locations A and B of these interactions, the quantities

$$E_\gamma = E_e' + E_\gamma'$$

$$\cos \varphi = 1 - \frac{m_o c^2}{E_\gamma'} + \frac{m_o c^2}{E_\gamma}$$

can be determined. The arrival direction of the infalling gamma ray is, therefore, known to lie on a cone mantle of half opening angle φ around the direction of the scattered gamma ray. The projection of the cone mantle on the celestial sphere is called the event circle.

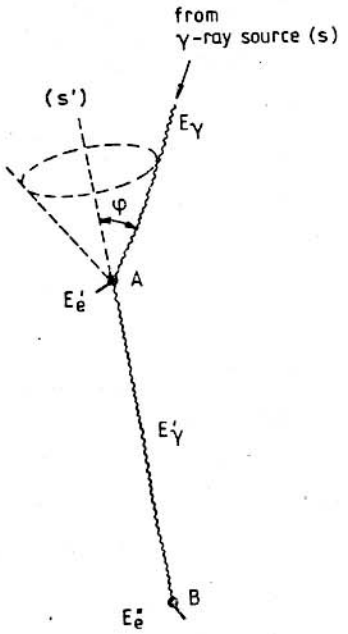

Fig. 8: Principle of measurement.

An astronomical object is identified by the intersection of different event circles arising from gamma rays from this object. If the scattered gamma ray of energy E_γ' is not totally absorbed, a wrong event circle is obtained. The circle will not contain the direction of the corresponding astronomical objects and, therefore, will not intersect with the circles of totally absorbed events. Events in which the gamma ray is not totally absorbed only increase the number of background events.

The energy resolution of this device for an astrophysical object is automatically good because only totally absorbed events are accepted for a source.

The advantage of the Compton telescope with its imaging properties within a broad field of view compared with shielded detectors widely used in low energy gamma ray astronomy is evident. Whereas "source on - source off" observations at different times are necessary for these shielded detectors in order to identify a source, different regions of the sky are observed simultaneously with an imaging system. "Source on - source off" observations at different times present problems onboard a satellite where the background will change with the position around the orbit.

The proposed Compton telescope is an improved version of a new balloon experiment at the Max-Planck-Institut, which was flown for the first time in October 1977 from Palestine, Texas. A photograph of the detector is shown on the reverse of the title page and is a more sophisticated instrument than the Compton telescope previously flown in 1973 and 1974. Whereas the detector elements and the size are nearly the same for both experiments, the angular resolution of the proposed version has been improved by a factor of 2.5 to 4. As outlined in the chapter on scientific objectives, an angular resolution of 3^o is mandatory to perform low energy gamma ray astronomy. This resolution will be provided by the proposed experiment.

2.2 Description of the Telescope

A schematic drawing of the telescope is shown on the cover. The telescope consists of two large area scintillation detectors, an upper one in which the infalling gamma ray is Compton scattered, separated by 1.5 m from a lower one , in which the scattered gamma ray is absorbed. Both detectors are nearly entirely surrounded by a thin anti-coincidence shield of plastic scintillator, which rejects charged particles. Between both detectors are four small plastic scintillation detectors containing weak Co^{60} sources; these are used as gamma ray calibration sources which can be electronically gated.

Upper detector (D1): It consists of 120 individual aluminum tanks of liquid scintillator NE 213 (See Figure 10). Each tank is of 6 x 6 cm^2 area and 15 cm depth and viewed by one 5 cm photomultiplier (RCA 8575). The total geometrical area of the upper detector is 4200 cm^2.

Lower detector (D2): A bottom view is shown in Figure 10. It consists of 14 cylindrical blocks of polycrystaline NaI(Tl) (Poliscin 1) of 7.5 cm thickness and 28 cm diameter, which are mounted on a groundplate within a diameter of about 1.50 m. Each NaI-block is seen from below by seven 7.5 cm multipliers (EMI 9821 B). The total geometrical area of the lower detector is 8620 cm^2.

Anticoincidence shields: Each shield consists of two 1.5 cm thick domes of plastic scintillator NE 110 (see Figure 10). Each dome is viewed by 24 photomultipliers (RCA 7151).

Calibration detectors: Each detector consists of a cylindrical piece of Co^{60}-doped plastic scintillator of 5 mm thickness and 1 cm diameter which is seen by a 1.9 cm photomultiplier (RCA C 70102 M).

Required gamma ray event parameters: A gamma ray is electronically identified by a delayed coincidence between the upper and the lower detector, combined with the absence of a veto from all charged particle shields and from the calibration detectors. The quantities measured for each event are as follows:

1. The energy of the Compton electron in the upper detector E_e' ($E_e' > 50$ keV);
2. The location of the collision in the upper detector;
3. The pulse shape of the scintillation pulse in the upper detector;
4. The energy loss E_e'' in the lower detector ($E_e'' > 500$ keV);
5. The location of the collision in the lower detector;
6. The pulse shape of the scintillation pulse in the lower detector;
7. The time of flight of the scattered gamma ray from the upper to the lower detector;
8. The absolute time of the event.

The quantities E_e' and E_e'' and the locations of the scattering processes in both detectors determine the energy and angular resolution of the telescope. The pulse shape measurements and the time-of-flight measurements are performed in order to reject background events and to protect against pulse pile-up.

In addition to this normal double scattering measuring mode the large area NaI-crystal of the telescope can and will be used to register gamma ray bursts and solar flares and to measure their energy spectra.

2.3 Electronics

The functions of the experiment electronics are shown schematically in Figure 9 and, starting with the detectors and proceeding through to the spacecraft interface, the functions are briefly described below.

In each detector element, the high voltage units (HV) associated with a group of photomultipliers (PM) may be switched on and off under relay command control.

In the upper detector D1 ten PMs are grouped together and two fast timing signals are derived from each group, one, D_{TU}, being an input to the time-of-flight (TOF) discriminator, the other, D_{PS}, being an input to the pulse shape discriminator (PSD). These are both located together with their associated time-to-digital converter (TDC) in the analogue electronics unit. In the lower detector D2 a fast timing signal, D_{TL}, is derived from each sodium iodide cell (each with 7 PMs) for TOF purposes.

A slow signal, obtained from a dynode of every PM of the D1 and D2 detectors (218 in total), is routed to the analogue electronics for pulse height analysis (PHA) and cell identification (ID).

A gamma ray event is initially selected according to coarse criteria established on the pulse heights of signals from D1 and D2, TOF, the absence of a veto signal (V) from all anticoincidence domes and provided no preceding interaction has deposited a large amount of energy in the triggered cell (overloads). If the initial event selection logic is satisfied, a series of actions are initiated: 1) PHA of the eight identified PMs of D1 and D2, plus the sum of the seven D2 PMs; 2) TDC of TOF and PSD; 3) the triggering of the digital electronics; and 4) the sampling of the event time.

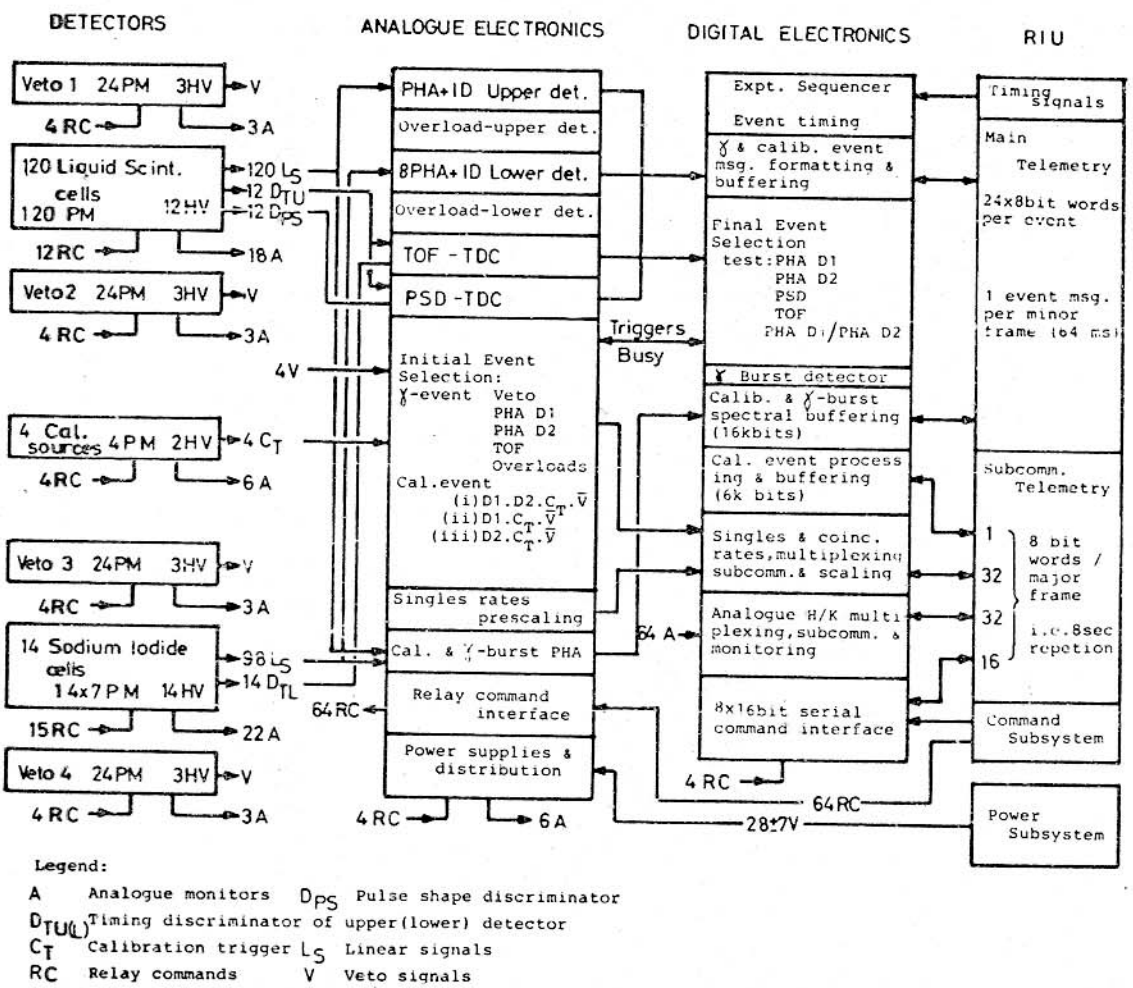

Fig. 9: Electronics Block Diagram.

The digital outputs of the analysis and the conversions are further checked against upper and lower limits, which are stored in the final gamma event selection logic via serial telecommands. The data are stored in the event buffer, with those events satisfying the final selection criteria having first priority and those failing one or more criteria having second priority for transmission through the telemetry.

The data from calibration events triggering D1 and D2 simultaneously are routed to the event buffer and transmitted through the telemetry as pseudo gamma events with third priority. 24 x 8 bit words are required per event message and one read out per minor frame (~ every 64 ms) is required. The effective maximum count rate of about 16 per sec is adequate for the expected gamma rate throughout the useful part of the orbit with a sufficient number of priority 2 and 3 events.

Rapid changes in counting rate, signifying possible gamma burst or solar flare events are detected within the digital electronics. Then, using a dedicated PHA, spectra from the sodium iodide cells are rapidly accumulated in a 16 K bit store for subsequent transmission using 1 x 8 bit words per minor frame (~ every 64 ms). To provide a diagnostic tool, the same PHA and 16 K bit store are used for full calibration spectral analysis of a selected PM.

Using a 6 K bit store, the average pulse height from every PM is continuously determined and transmitted at a slow rate, for additional routine monitoring. Single and coincidence counting rates required for scientific and housekeeping purposes, analogue housekeeping (voltage monitors, temperatures) in digital form and command monitoring require transmission through subcomm. telemetry with a total of 81 subcomm. channels required. The available 64 relay commands and 8 x 16 bit serial commands from one RIU are adequate for experiment control.

An estimate of the power requirement of the whole experiment has been made and with power supply converter losses taken into account shows that 100 watts are required.

2.4 Mechanical Design

The mechanical design of the telescope is illustrated in the drawings of Figure 10. The upper and lower detectors are mechanically separated with each detector being mounted directly on the base plate of the spacecraft (S.C.).

In the case of the upper detector, the liquid scintillator cell assembly is about 0.94 m x 1.22 m and fits with the charged particle shields inside the prescribed 1.7 m diameter. Each self-contained module (cell and PMT with associated circuitry) is held in position by truss-type beams, one on either side of each row of cell arrays. There is an additional similar truss beam through the center of the entire assembly, and two more beams to complete the sides of the assembly. The structural beams are angled away to avoid obscuration and scattering effects of gamma rays entering the scintillator cells within the opening angle of the telescope. A structural analysis by a subcontractor has indicated that the proposed design will have an adequate safety margin to survive exposure to the spacecraft environment.

The scintillating liquid will be contained in vessels especially designed to meet the S.C. mechanical specifications. Preliminary design considerations confirm that an adequate safety margin could be met by using a cell which is a dip-brazed integral assembly of aluminum plate stock 0.16 cm in thickness (Fig. 10). (Needle valves are used for venting and filling.) However, in the design development phase alternative methods of construction will also be evaluated. The machined opening for the PMT can be seen to be fitted with an O-ring of Viton A, against which a glass window is held in place by a threaded ring. This single cell concept is tentatively chosen to minimize the possibility of leakage of the scintillation liquid. The expansion chamber on the scintillator cell provides for the differential expansion of the aluminum shell and the NE213 liquid by means of a metal bellows integrally brazed into the cell adequate for the specified temperature range. Further details on the mechanical design of the upper detector can be found in the A.S.E. subcontract proposal (ASE-4245-1, 1978).

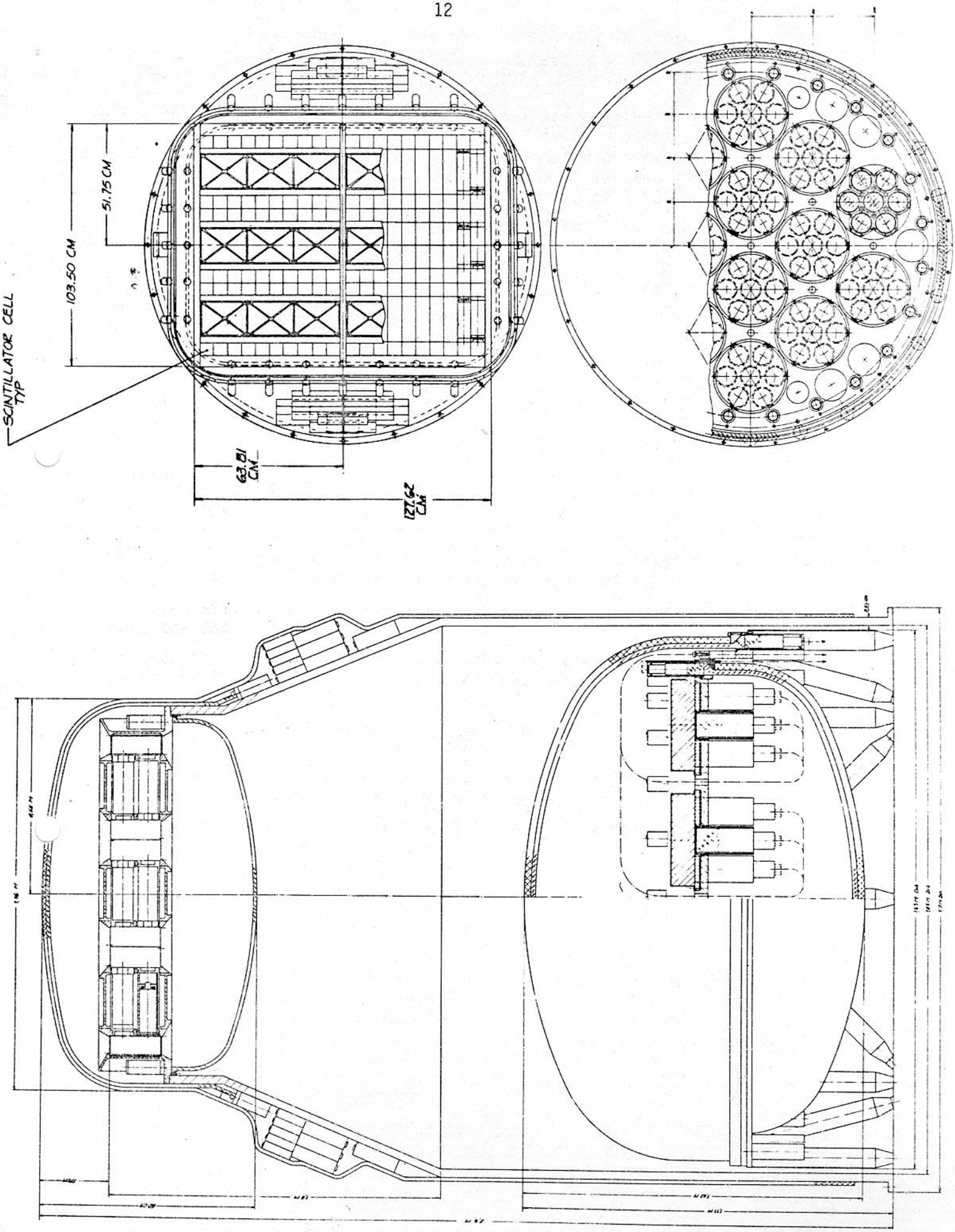

Fig. 10: Mechanical design.

In the lower detector the 14 Poliscin blocks are mounted on a ground plate of 1.50 m diameter in such a way that each block with its seven photomultipliers can be taken off as a unit without uncoupling the PM tubes and the associated electronics. The ground plate is directly connected to the plate of the S.C. The two anticoincidence charged particle domes are designed to fit inside a diameter of 1.63 m.

All four domes will be tested extensively both for light collection efficiency and capability to withstand mechanical vibration which could possibly produce crazing. A preliminary mechanical analysis indicates that the design of the assembly is adequate to withstand the expected loads on the spacecraft. The domes for the lower detector are circular in cross-section; whereas for the upper detector they are rectangular to reduce weight.

The experiment electronics will be contained in boxes placed on the base plate below the lower detector. The overall height of the experiment is 2.50 m and the estimated weight is 1.350 kg (upper detector: 480 kg including structure; lower detector: 750 kg; electronics: 30 kg; harness: 90 kg).

3. Instrument Performance

3.1 Requirements and Detector Performance

In order to achieve the scientific objectives of this experiment, the Compton telescope must have as a minimum the following capabilities:

1) The time-of-flight must be measured to provide directional information and reduce the detector background.
2) To reduce the neutron induced background, the capability must exist in the upper detector cells to separate neutrons from gamma rays. This is accomplished by pulse shape discrimination (PSD).
3) Individual Compton interactions must be located to an accuracy sufficient to achieve a 3^{o} angular resolution.
4) The telescope must absorb as completely as possible the scattered gamma ray and the individual elements must have the best possible energy resolution.
5) The upper and lower detector assemblies must be completely surrounded by an effective particle anticoincidence shield to eliminate the charged particle background.

The proposed detector achieves these capabilities in the following way.

Time-of-flight-measurement

The time-of-flight (TOF) measurement rejects those events which make the first Compton interaction in the lower detector and then scatter into the upper one and gamma cascades originating in the S.C. Figure 11 shows an actual TOF distribution observed in the 1977 balloon flight at 3.5 g/cm^2. It is clear that the TOF system achieved the required separation.

Pulse-shape measurement

The purpose of the pulse-shape measurement in the upper detector is to reject neutron induced events. This necessity for pulse-shape discrimination requires the selection of a liquid scintillator (i.e. NE 213, which has excellent pulse-shape properties), because plastic scintillators cannot be used for PSD. Neutrons can simulate Compton scattering events if they undergo reactions of the type $(n,n'\gamma)$ or $(n,x\gamma)$ with the carbon in the upper detector (x is a charged particle e.g. proton or α-particle). When the pulse in the upper detector is produced by a proton or heavier particle, it can be

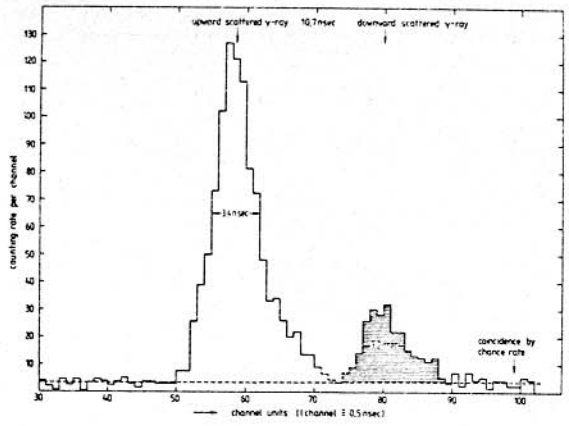

Fig. 11: Actual TOF distribution scaled to 1.5 m separation.

PSD on the upper detector (see page 19). The pulse shape measurement in the lower detector is performed in order to recognise pile-up effects resulting from high counting rates and the long decay time ($\sim$ 200 ns) in the NaI.

Location of the scattering process

In order to achieve an angular resolution for the Compton telescope of $\sim 3^0$, the location* of the scattering points has to be determined more accurately than in the case of the MPI-balloon experiment, where the accuracy is determined by cell sizes of 15 x 15 cm^2.

For the upper detector the improvement is achieved by using smaller cell sizes (6 x 6 cm^2). In the lower detector the improvement is achieved by applying the principle of the Anger camera. The size and shape of the lower detector elements represent the best choice between electronic complexity, mechanical design considerations, total absorption and spatial resolution. The location of the scattering point within the NaI-block (28 cm diameter) is derived from the relative pulse heights of the seven PM's. The accuracy that can be obtained is shown in Figure 13. The 1-sigma uncertainty of the true scattering point was determined from laboratory measurements at 0.662 MeV on a 20 cm diameter crystal of the same thickness (Gumplinger, 1978). These values were multiplied by a factor of 1.4 for the 28 cm crystal. At higher energies the spatial resolution improves rapidly but is limited by the spread due to multiple scattering of the infalling gamma ray in the NaI-block. This was confirmed by computer simulations (Mitchell, 1977).

distinguished from electrons in Compton events by PSD. Figure 12 demonstrates clearly how gamma and neutron induced events can be separated by this means. For electron energy losses above 1 MeV the neutron rejection is better than 99%. It falls to 94% between 100-200 keV. If neither the particle n' nor x produces a signal in the upper detector but the gamma ray makes a real double scattering, then the resulting event cannot be distinguished from a real gamma ray event. These events have to be tolerated and produce an intrinsic detector line at 4.4 MeV. (C^{12} anregung)

It should be emphasised that determination of the diffuse cosmic gamma ray component is impossible without

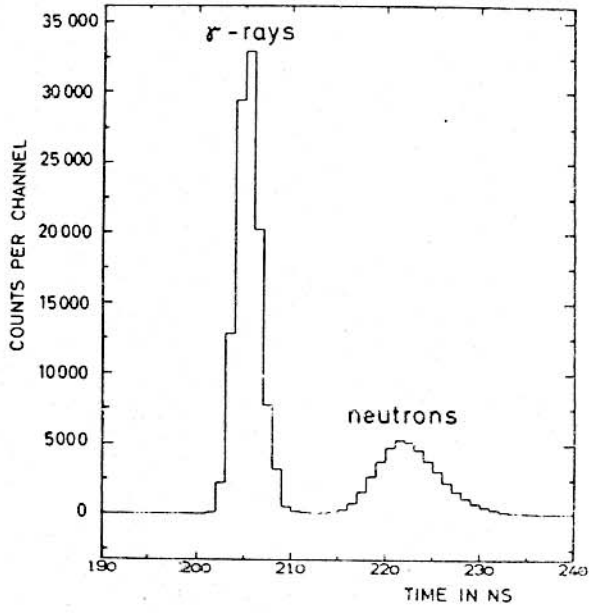

Fig. 12: Separation between gamma ray and neutron events in the upper detector by PSD (E_e' = 1-2 MeV).

Energy resolution of the scintillation detectors

The energy and angular resolution of the Compton telescope are both determined by the energy resolutions of the upper and lower detectors. These are known from laboratory measurements. For a broad parallel beam of infalling 4.41 MeV gamma rays the measured

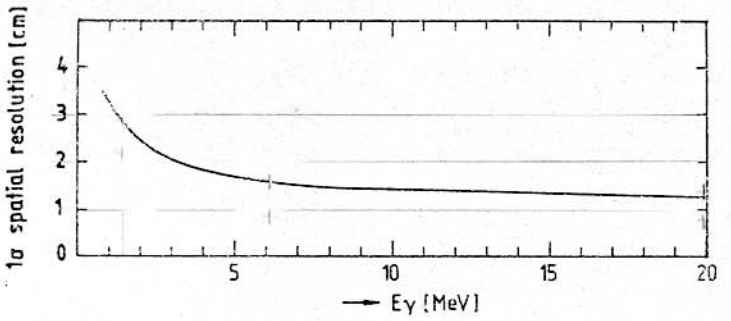

Fig. 13: 1σ-spatial resolution of the lower detector.

3.2 Derived Properties of the Telescope

Results from several balloon flights have shown that the performance of a Compton telescope can be accurately predicted from the known characteristics of the individual detector elements. The powerful aspect of the proposed Compton telescope is its imaging properties. For each specific investigation (e.g. diffuse cosmic, point sources, etc.) the best combination of efficiency, energy resolution, angular resolution and, as a result, overall sensitivity can be chosen at the stage of data analysis by applying the appropriate selection criteria to the gamma ray events. In the following sections the performance parameters are derived for a typical set of selection criteria.

Angular resolution

Figure 8 illustrates the reconstruction of the direction of gamma rays in the plane defined by the primary and scattered gamma ray (γ,γ'). The projection of the measured direction of γ (AB) on the sky is S'. The angular resolution, being the uncertainty (σ_φ) in the derived angle SAS' is composed of two uncertainties: 1) σ_S, the uncertainty in AB, defined by the combined spatial resolutions in A and B (in the same plane) and their separation d; 2) σ_E, the uncertainty in the measured angle φ, defined by the energy resolution in A and B. Because σ_S and σ_E are independent, $\sigma_\varphi^2 = \sigma_S^2 + \sigma_E^2$. The probability distribution for the true position of S forms an anulus on the sky (event circle) centered on S', radius φ and a width defined by σ_φ.

Using the Compton scattering formula,

$$\sigma_E^2 = \frac{1}{(\sin\varphi)^2}\left[\left(\frac{mc^2}{E_{\gamma'}^2} - \frac{mc^2}{E_\gamma^2}\right)^2 \sigma_{E_{\gamma'}}^2 + \left(\frac{mc^2}{E_\gamma^2}\right)^2 \sigma_{E_{e'}}^2\right],$$

where $\sigma_{E_{\gamma'}}$ and $\sigma_{E_{e'}}$ represent the 1-σ energy resolution in B and A, respectively. It should be noted that σ_E is not very dependent on φ.

The spatial resolution in B (σ_B) is given in Figure 13. The uniform distribution of the scatter point A in the 6 cm cells may be approximated by a gaussian distribution

energy resolution of a prototype cell in the upper detector is 9.2% for a 3 MeV energy loss (see Figure 14). For the NaI detector the resolution is 10.4% FWHM at 662 keV.

Anticoincidence shield

Experience with similar anticoincidence counters on previous balloon experiments has shown that the required efficiency of 99.9% can easily be achieved.

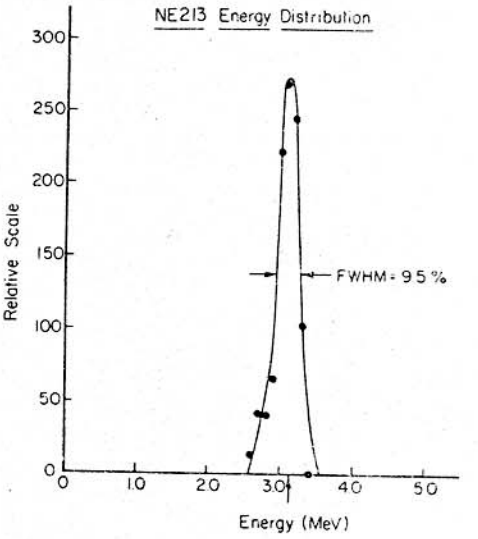

Fig. 14: Energy resolution of an upper detector cell at E'_e = 3 MeV.

with $\sigma_A \simeq 2.0$ cm. Hence,

$$\sigma_S^2 = \frac{1}{d^2} (2.0^2 + \sigma_B^2).$$

The resulting values of σ_S, σ_E and σ_φ, averaged over the distribution of scatter angles, are given in Figure 15.

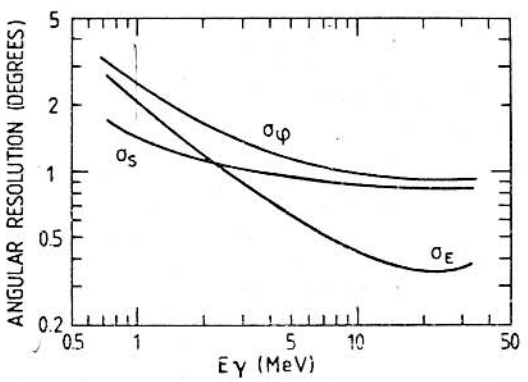

Fig. 15: Angular resolution (FWHM) of the proposed Compton telescope.
σ_S : contribution from spatial resolution
σ_E : contribution from energy resolution
σ_φ : total angular resolution.

These are confirmed by a Monte Carlo calculation, in which all possible interaction processes of the infalling and scattered gamma rays (photoeffect, Compton effect, pair production) and of the secondary electrons and positrons (ionization, Coulomb scattering, bremsstrahlung, annihilation) were taken into account. In addition, the statistical fluctuations of the pulse height measurements with photomultipliers were also included.

Figure 16 shows the results of the simulation of monoenergetic celestial gamma ray soures of 5 MeV. In Fig. 16 the telescope axis was pointed at $(0^o,0^o)$. For each bin the number of event circle intersections n_i was determined. The bins with $n_i \geq 1/2\ n_{max}$ and $n_i \geq 1/10\ n_{max}$ are marked differently (n_{max} is the largest number of intersections per bin).

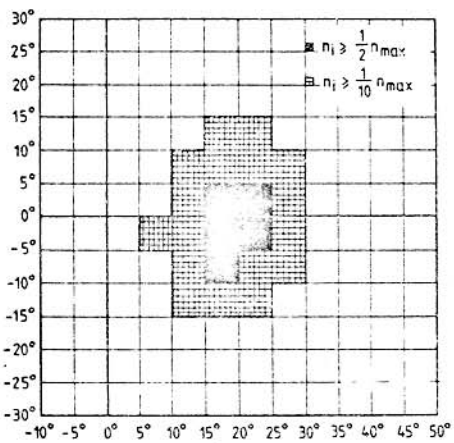

c

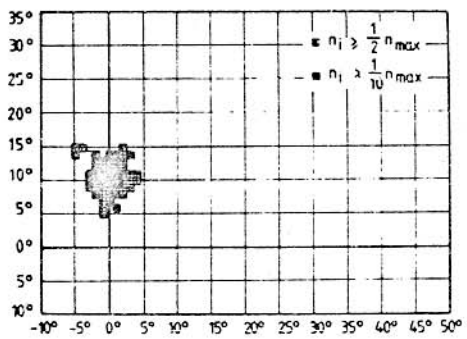

a

10°/10°

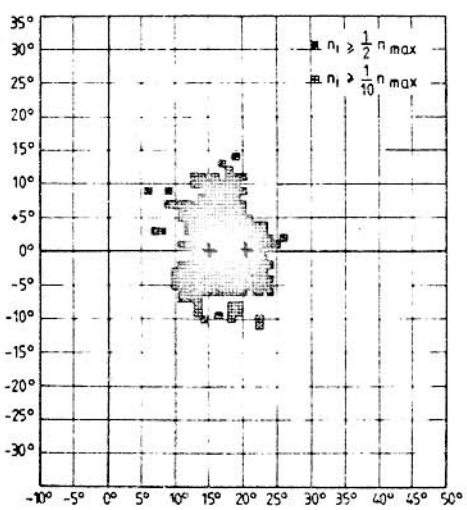

0°/15°
+
0°/20°

b

Fig. 16: Resolution of the telescope obtained from a Monte Carlo simulation of a 5 MeV celestial gamma ray source.
(a) and (b) are for the proposed Compton telescope, (c) is for the MPI-balloon telescope. (In each case 200 events were simulated.)

For Figure 16a the source was assumed to be at (10^0, 0^0) and for Figure 16b, two sources of equal intensity were taken at (0^0, 15^0) and (0^0, 20^0). It is clear that the proposed telescope can resolve the two sources at a separation of 5^0.

In order to demonstrate the improved angular resolution obtained in the proposed telescope, the same calculations have also been performed for the MPI-balloon experiment (upper and lower detector elements: 15 x 15 cm^2, separation: 1.2 m) and are shown in Figure 16c. The improvement with the proposed detector at 5 MeV is nearly a factor of 4.

Energy resolution

The energy resolution of the telescope is determined by the resolution of both detectors. Figure 17a shows the energy spectrum obtained with the MPI-balloon experiment from a Na^{24}-gamma ray source (1.35 MeV and 2.75 MeV) above the telescope axis if all triggered events are accepted. In the case of an astronomical object the Compton tail of the gamma ray line can be practically suppressed if only events within 2 σ_{co} of the source are accepted (the black bins in Fig. 16). This is due to the fact that only totally absorbed events are inside the resolution element. Figure 17b shows the result of a Monte Carlo simulation in which the energy spectrum from a monoenergetic celestial gamma ray source at 2.75 MeV was determined. The resolution (FWHM) at 2.75 MeV is 8%.

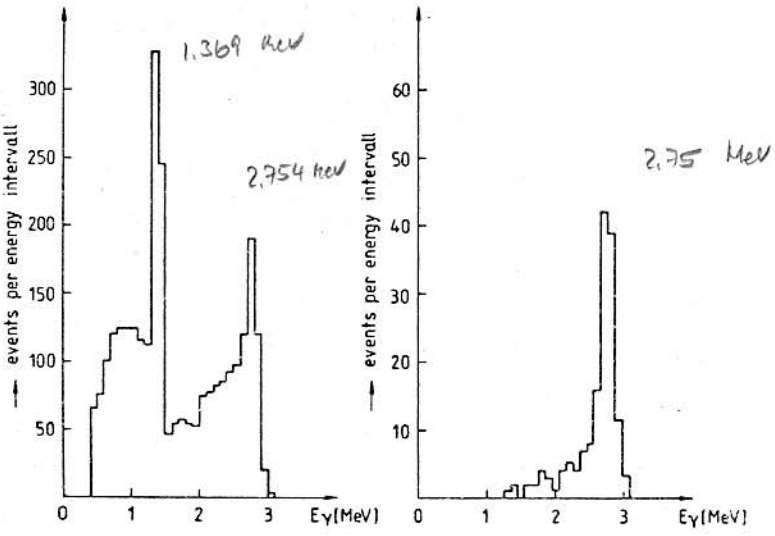

Fig. 17: Energy resolution of the MPI-balloon telescope. (a): measured Na^{24}-spectrum, all events are accepted. (b): 2.75 MeV-line profile from a simulated astronomical object if only events inside the angular resolution element of the source are accepted.

Sensitive area

Figure 18a and b give the sensitive area and geometrical factors as a function of energy calculated with the same Monte Carlo program (see section 3.2: angular resolution). These data refer only to totally absorbed events, for which the correct directional assignment is obtained. The wide effective field of view is clearly illustrated in Fig. 18c.

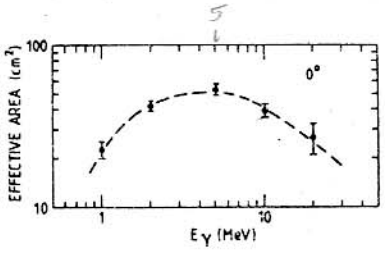

Fig. 18a: Sensitive area for vertical incidence.

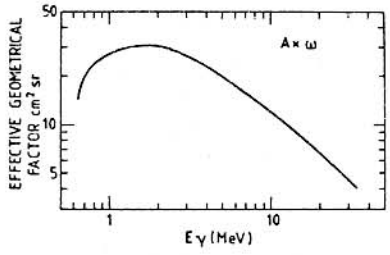

18b: Effective geometrical factor.

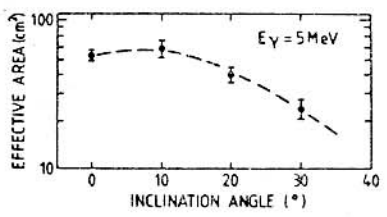

18c: Sensitive area at 5 MeV as a function of off-axis angle.

Polarization

If the infalling gamma radiation from an astronomical object is linearly polarized, the scattered gamma ray will be found in the lower detector preferentially in the plane which is perpendicular to the vector of polarization. In Figure 19 the ratio $P_\perp/P_\parallel$ is plotted as a function of energy for three different scattering angles: $\varphi = 20^0$, 30^0 and 40^0. ($P_\perp$ and $P_\parallel$ are the probabilities of being scattered perpendicular or parallel to the vector of polarization.)

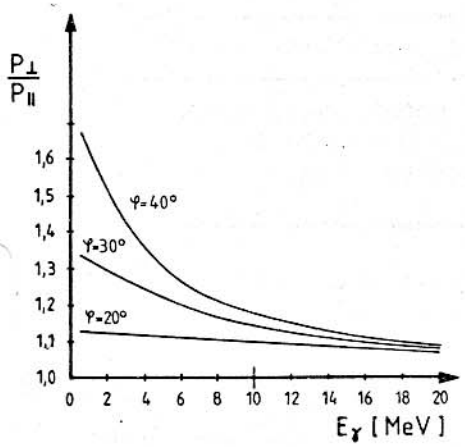

Fig. 19: Intensity ratio $P_\perp/P_\parallel$ for linearly polarized infalling gamma radiation derived from the Klein-Nishina formula.

Background radiation

The sensitivity of the Compton telescope to be flown on the GRO satellite is critically dependent upon the background produced by the environmental radiation. The individual contributions to the background counting rates are analyzed in detail in the following sections:

1. Gamma rays from the S.C. structure and adjacent experiments

   a) Double scattering events:

   Background gamma rays that scatter from the lower to the upper detector are rejected by the TOF measurement. Since the radiation from the surrounding masses are all outside a cone of half angle 80^0 centered on the telescope axis, double scattering events caused by these background gamma rays are rejected by the usual event selection criteria.

   b) Chance coincidences:

   From the individual count rate spectra of the upper and lower detectors the spectrum of the chance coincidence rate can be calculated. The count rate spectrum in the NaI detector is estimated from measurements aboard Apollo 15 (interplanetary space) and aboard OSO-1 (an orbit similar to the GRO orbit) (Peterson, 1965, 1975). As shown in Figure 20, the count rate spectrum in the earth orbit is a factor of below that in interplanetary space. The gamma ray spectrum measured on Apollo 15 was found to be quite similar to that on a typical balloon flight. In the upper detector the count rate spectrum obtained from balloon measurements with the MPI Compton telescope was reduced by the same factor of 3 to obtain the expected count rate spectrum for the upper detector in the GRO orbit.

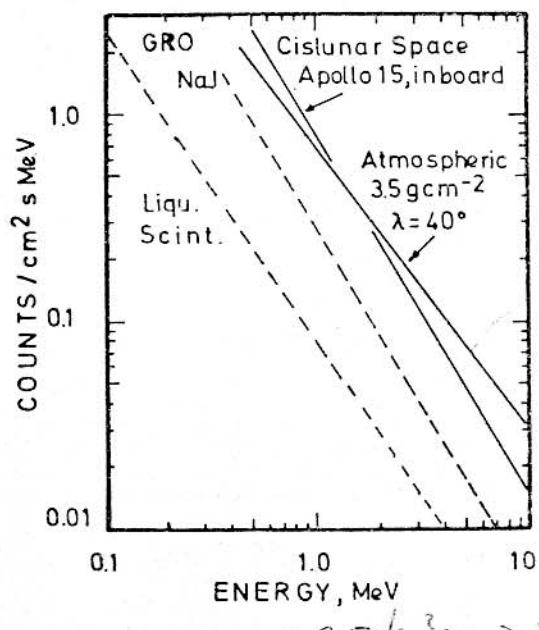

Fig. 20: Comparison of gamma ray count rates of a NaI-crystal on Apollo 15, at balloon altitudes and on GRO, and the estimated count rate of the liquid scintillator on GRO.

The resulting count rate spectra are then:

upper detector: $\propto E^{-1.46}$, integral $E \geq 50$ keV: 4.1×10^3 cts/s

lower detector: $\propto E^{-1.71}$, integral $E \geq 500$ keV: 4.3×10^3 cts/s

Applying the event selection criteria the resulting energy distribution of the chance coincidence rate is:

Energy interval (MeV)	1-2	2-3	3-5	5-10	10-30
Chance coincidence rate (% of diffuse cosmic gamma ray rate)	3.3 %	3.9 %	7.7 %	17 %	25 %

The actual contribution from chance coincidence will be very accurately determined from the measured TOF distributions.

c) Cascade gamma rays:

If a single nucleus emits simultaneously more than one gamma photon, the upper and lower detectors could be triggered by single interactions. The time difference between the triggerings depends upon the position of the radiating material. The most intensive of the cascade gamma rays are produced in the reaction ^{27}Al (n,α) Na^{24} which yields two gammas at 1.37 and 2.75 MeV. The estimated contribution from this process in the S.C. and neighbouring experiments is small because of the TOF requirement and of the small solid angle subtended by the telescope. More important is the activation in the Compton telescope structure itself which will be discussed in 3c.

Neutron induced reactions in the detector

a) Continuum gamma ray spectrum:

Reactions of the type (n, n'γ) and (n,xγ) in the upper scintillator have been considered by Daugherty and Schönfelder (1977) to determine the Compton telescope background in a balloon flight environment. The neutron flux on GRO at the upper detector (estimated from Apollo-Soyuz ASTP measurements) is 1 n/cm^2 s above 20 MeV (10 x the atomospheric value) and 0.5 n/cm^2 s for 1-20 MeV (2.2 x the atmospheric value). These are conservative neutron flux values.

The resulting background gamma ray rate on GRO relative to the diffuse cosmic rate before and after application of pulse shape discrimination is:

Energy interval (MeV)	1.5-2.0	2-3	3-5	5-10
neutron induced rate (before PSD)	80 %	170 %	440 %	2000 %
rejection probability of PSD	0.90	0.95	0.98	0.995
neutron induced rate (after PSD)	8.0 %	8.5 %	8.8 %	10.0 %

b) Neutron induced gamma ray lines:

The reaction C^{12} $(n,n'\gamma)$ C^{12} produces the 4.43 MeV gamma ray line in the upper detector as discussed in section 3.1 on pulse shape discrimination. In addition, thermal neutrons produce a gamma ray line at 2.23 MeV via the reaction H^1 (n,γ) H^2.

From the balloon flights with the MPI Compton telescope upper limits for the line fluxes were derived at balloon altitudes and an estimate for GRO was made using the higher neutron fluxes in orbit.

3. Activation gamma rays

a) Activation in the lower detector (NaI):

The TOF system rejects gamma rays from the lower detector.

b) Activation in the upper detector (liquid scintillator):

Two proton induced activations dominate:

$C^{12}(p,pn)C^{11} \xrightarrow{20.3\ m} B^{11} + \beta^+(E = 0.96\ MeV)$, $(\beta^+ + \beta^- \rightarrow 2\ \gamma)$.

$C^{12}(p,p2n)C^{10} \xrightarrow{19.4\ s} B^{10} + \beta^+(E = 1.87\ MeV) + \gamma\ (0.717\ MeV)$, $(\beta^+ + \beta^- \rightarrow 2\ \gamma)$.

The event selection criteria will reject gamma ray events caused by the first reaction, whereas the second reaction presents no problem because of the short half-life and small cross-section.

c) Activation in structure close to the upper detector:

The mass of the Al structure surrounding the upper detector is ~ 90 kg, of which ~ 3 kg are in the field of view of the telescope. The neutron reactions producing gamma rays that have been considered are: thermal neutron capture, inelastic neutron scattering, (n,p) and (n,γ) reactions with subsequent decay of the produced nuclides.

Cross sections for these reactions have been compiled by Young and Foster (1972). The thermal neutron flux in the S.C. is estimated to be 0.5 n/cm^2s and the flux between ~ 3 and 25 MeV is ~ 0.5 n/cm^2s. It must be noted that for single photon emission only the mass of Al in the field of view contributes to the background rate, whereas for cascade emission (Na^{24}) the total mass around the detector can cause triggers as described in the section on cascade gamma rays. The expected background fluxes from these processes are included in Figure 6, which was presented in the section on scientific objectives. This neutron induced background in orbit will be accurately determined with the experience gained from pre-launch calibrations at accelerators, neutron intensity measurements in orbit and theoretical model calculations.

A summary of all background contributions is shown in Figure 6. The diffuse cosmic gamma ray spectrum was taken from Schönfelder (1977). The counting rates in the upper and lower detectors and the anticoincidence shields have also been calculated using estimated proton fluxes of $1/cm^2s$ and secondary electron fluxes (produced in satellite mass) of $1/cm^2s$ and the above quoted neutron fluxes. The rates are typically 20 000 counts/s.

3.3 Detection Sensitivity and Expected Results

Using the derived telescope properties the sensitivity for the detection of point sources and for extended features like the galactic plane, can be calculated in a straight forward manner. Appendix I gives a detailed account of the parameters affecting these sensitivities. In the calculation it was estimated that for a fixed pointing of the S.C. only 50% observation time remains as a result of earth occultation and passage through the radiation belts. Results are summarized in the table on page 22.

The power of the proposed instrument is further illustrated in Figures 1, 3 and 7 which show typical sensitivities in comparison with reported intensities and current predictions.

It is appropriate to underline the following points:

1. Accurate spectral data will become available for all sources down to the quoted sensitivity limits.
2. In the particular case of pulsars, provided the period is well known, even better sensitivity will be obtained depending on the pulsar duty cycle.
3. Sources above the sensitivity limit can be effectively studied for possible time variability. For instance, variability at a level of about 10% of the Crab intensity on a time scale of a day cannot escape detection. The suggestion that the apparently high fluxes reported in this energy range may, at least in some cases, reflect time variability, can easily be checked down to a timescale of 10^3s.
4. Point sources detected at the 5-σ limit will be located within a 90% confidence level error radius of 30 arc min and proportionally better for stronger sources. This will provide a strong basis for establishing identification on positional grounds with e.g. hard X- or high energy gamma ray sources.
5. The determination of the absolute spectrum of the diffuse cosmic gamma ray spectrum requires a final correction for instrumental background. The instrument itself provides the data to make this correction accurately. The time-of-flight and pulse shape spectra accumulated from all detected events give full information on the remaining number of background events after the event selection criteria have been applied (see Figure 11). In addition, the pulse shape measurement allows one to specifically investigate the effects caused by neutron interactions in the upper detector. This, combined with the foreseen calibration of the detector in neutron beams, also provides a firm basis for the corrections required for other neutron reactions. Finally, any instrumental background carries a clear signature, namely its dependence on geomagnetic latitude. The validity of the correction procedure may thus be confirmed by the absence of similar variability in the derived cosmic flux. Therefore, the accuracy of the measurement of the diffuse cosmic flux will reach the experiment calibration accuracy, for which a 10% level is obtainable. The proposed experiment will give a definite answer whether the excess in the MeV-range is indeed of cosmic origin.

4. Observation Programme

With the proposed instrument a complete sky survey to the quoted sensitivity level could be achieved with 24 pointings of one month duration each. The scientific objectives illustrate the importance of detailed investigations of the following objects and regions: high energy gamma ray sources, bright or hard X-ray sources, specific extragalactic sources, the galactic plane, high galactic latitude regions and the sun. In general, all these objects will be of equal interest to other experiments on board GRO.

It is premature to assign priorities to specific observations although an early survey of the galactic plane, lasting say 2 months, could be beneficial in maximizing the total scientific return from the mission.

Comptel Detection Sensitivities

5 σ confidence levels

Type of observation	Point Sources		Galactic Survey	
	One month pointed observation[1] $T = 1.3\times10^6$s	Accumulation $T = 10^3$s	One month pointed observation[1] $T = 1.3\times10^6$s	
			Integrated over $\Delta l^{II} = 20^o$	Integrated over $\Delta l^{II} = 5^o$
Objectives	Deep survey, spectra, locations, variabilities	Flare phenomena	Detailed spectra	Detailed structure
Energy range (MeV) Continuum	$(cm^{-2}s^{-1}MeV^{-1})$	$(cm^{-2}s^{-1}MeV^{-1})$	$(cm^{-2}s^{-1}rad^{-1}MeV^{-1})$	$(cm^{-2}s^{-1}rad^{-1}MeV^{-1})$
1-2	4.6×10^{-5}	2.1×10^{-3}	1.7×10^{-4}	6.1×10^{-4}
2-5	1.0×10^{-5}	4.5×10^{-4}	3.6×10^{-5}	1.3×10^{-4}
5-12	1.2×10^{-6}	9.6×10^{-5}	5.1×10^{-6}	1.8×10^{-5}
12-30	1.8×10^{-7}	5.4×10^{-5}	8.8×10^{-7}	3.1×10^{-6}
1-30	$\frac{dI}{dE} = 5.0\times10^{-5}E^{-2}$	$\frac{dI}{dE} = 2.6\times10^{-3}E^{-2}$	-	-
Lines	$(cm^{-2}s^{-1})$	$(cm^{-2}s^{-1})$	$(cm^{-2}s^{-1}rad^{-1})$	$(cm^{-2}s^{-1}rad^{-1})$
0.8	3.2×10^{-5}	3.3×10^{-3}	1.1×10^{-4}	4.1×10^{-4}
2.2	1.8×10^{-5}	1.0×10^{-3}	6.6×10^{-4}	2.4×10^{-4}
4.4	7.2×10^{-6}	6.5×10^{-4}	2.9×10^{-5}	1.0×10^{-4}
6.1	2.8×10^{-6}	5.0×10^{-4}	1.2×10^{-5}	4.0×10^{-5}
Polarization	$(cm^{-2}s^{-1}MeV^{-1})$			
1-5 (3σ)	$\frac{dI}{dE} = 8 \times 10^{-4}E^{-2}$			

[1] Similar sensitivities will be reached for each point in the sky if pointing directions are more or less evenly distributed over the sky during the two years lifetime of GRO.

It has been earlier noticed that the pointing mode of operation results in a loss of observation time due to earth occultation. It may be suggested to investigate the possibility of an anti-earth scanning mode of operation. This would result in increased observation time and in a more uniform sky coverage.

5. Calibration and Data Analysis

Comprehensive pre-launch calibrations will be performed in order to determine the sensitive area of the Compton telescope and its angular and energy resolution. The entire energy range of the telescope can be covered using radioactive gamma ray sources and gamma ray lines from proton-induced de-excitation reactions. The table lists the easily available energies.

Source	Energy (MeV)
Mn^{54}	0.835
Co^{60}	1.17, 1.33
Na^{24}	1.35, 2.75
Am^{241}/Be^{9}	4.4
$F^{19}(p,\gamma)Ne^{20}$	6.1, (7.1)*
$B^{11}(p,\gamma)C^{12}$	12.1, 16.1
$Li^{7}(p,\gamma)Be^{8}$	17.6, (14.7)*
$T(p,\gamma)He^{4}$	19.8

aus Diss. Herterich

*significantly weaker accompanying line.

The calibration results will be cross checked against and supplemented by detailed Monte Carlo simulations. Further the response of the telescope to background radiation will be investigated at proton and neutron beams.

Data analysis

The comprehensive evaluation of the Comptel data requires a sophisticated approach. Overall management of the data analysis will be exercised throughout the programme. An even distribution of software and data analysis tasks will be made, based on well defined interfaces between the institutes. The timely software development, qualified through the analysis of simulated and calibration data, will safeguard full hardware and software compatibility.

On orbit data reduction tasks amount to assessment of scientific and technical performance and final analysis of the flight data.

Great value is seen in implementing a selection of programmes used in the final analysis in a system to which a meaningful sample (10-30%) of the data can be made available within a relatively short time (~ days). Such a system may be used for routine monitoring of the scientific performance of the experiment and provides the means to keep the instrument performance at its best. In addition, the overall scientific return of the mission can be enhanced by taking into account preliminary conclusions in planning the future observation programme and through the early announcement of any significant discovery to the scientific community.

6. Management Summary

The following is a summary of the relevant chapter which appears in the management section of this proposal. As all team members are scientists or engineers of established reputation, only 2 relevant bibliographical references for each are given.

Max-Planck-Institut für extraterrestrische Physik:

V. Schönfelder, PI, Head of Low Energy Gamma Ray Astronomy Group; cosmic ray neutrons; gamma ray astronomy balloon experiments; responsible for the lower detector.

"Diffuse Cosmic and Atmospheric MeV Gamma Radiation from Balloon Observations", Ap. J. 217, 306 (1977).

"The MPI Imaging Double Compton Telescope for Observations of MeV Gamma Radiation", Proc. 12th ESLAB-Symp., ESA SP 124, 301 (1977).

F. Melzner, Staff Member; ionospheric physics, magnetospheric physics; rocket experiments; GEOS; Experiment Manager.

"Instrument to Define the Drift Velocity of the Plasma, GEOS-Experiment S329", (in German), Zeitschrift für Flugwissenschaften 1, 303 (1977).

"The GEOS-Electron Beam Experiment S329", to be published in Space Science Instr. (1978).

G. Kanbach, Staff Member; neutrons; gamma rays; balloon experiments; OSO-7; COS-B; Experiment Scientist.

"Support for CRAND Theory from Measurements of Earth Albedo Neutrons between 70 and 250 MeV", J.G.R. 79, 5159 (1974).

"COS-B Results on a Search for Pulsed Gamma Ray Emission from Radio Pulsars", ESA SP 124 (1977).

Cosmic Ray Working Group, Leiden University:

B.N. Swanenburg, Co-PI, Director CRWG; X- and gamma rays; cosmic rays; balloon and rocket experiments in X-ray astronomy; OGO-5 and COS-B; responsible for analogue electronics; Experiment Manager.

"Energy Dependent Time Lag in the Long-Term Modulation of Cosmic Rays", J.G.R. Vol. 78, No. 1, 292 (1973).

"New High Energy Gamma Ray Sources Observed by COS-B", Nature 269, 494 (1977).

W. Hermsen, Staff Scientist; gamma ray astronomy; COS-B; Experiment Scientist.

"COS-B Observations of Pulsed Gamma Ray Emission from PSR 0531+21 and PSR 0833-45", Astron. Astrophys. 61, 279 (1977).

"New High Energy Gamma Ray Sources Observed by COS-B", Nature 269, 494 (1977).

J.A.M. Bleeker, Staff Scientist; balloon and rocket experiments in X-ray astronomy; EXOSAT co-experimenter; Support to Experiment Manager.

"The Diffuse Soft X-Ray Sky", Space Science Reviews, Vol. 20, No. 6, 815 (1977).

"Soft X-Ray Spectra of the Cygnus Loop and Cygnus X-2 in the Energy Range 0.16-6.7 keV", Ap. J. 178, 377 (1972).

A.J.M. Deerenberg, Staff Scientist; balloon and rocket experiments; X-ray astronomy; Support to Experiment Manager.

"Soft X-Ray Spectra of the Cygnus Loop and Cygnus X-2 in the Energy Range 0.16-6.7 keV", Ap. J. 178, 377 (1972).

"Features in the Brightness Distribution and Spectra of the Soft X-Ray Background", Astron. Astrophys. 48, 235 (1976).

University of New Hampshire Personnel:

J.A. Lockwood, Co-PI; Professor of Physics; galactic cosmic rays; atmospheric neutrons and gamma rays; Investigator on AF Discoverer satellites and OGO-6; responsible for upper detector assembly.

"Energy Spectrum and Flux of High Energy Neutrons at Balloon Altitudes", J.G.R. 81, 6211 (1976).

"Flux and Energy Spectrum of Atmospheric Neutrons and Gamma Rays", to be published in J.G.R. (1978).

W.R. Webber, Professor of Physics; gamma rays and X-rays; galactic and solar cosmic rays; Investigator on OGO-2 and 4; Pioneer 8, 9, 10, 11; Voyager 77; responsible for charged particle shield design and construction for upper detector assembly; Experiment Scientist.

"Pioneer 10 Measurements of the Differential and Integral Cosmic Ray Gradient between 1 and 3 Astronomical Units", Ap. J. 185 (1973).

"Hard X-Ray Spectra of Galactic Sources", 14th Intern. Cosmic Ray Conf., Munich (1975).

L.A. Frieling, Engineer/Pyhsicist; Engineer for rocket and balloon payloads for neutron and gamma ray detectors 1963-1977; chief project engineer (Experiment Manager) for the upper detector assembly. (See publication listed under J.A. Lockwood)

Space Science Department of ESA:

B.G. Taylor, Co-PI; Head of High Energy Astrophysics Division; gamma ray astronomy; cosmic rays; X-ray astronomy; Experimenter on OGO-5; HEOS-1/2 and COS-B; Payload Manager of EXOSAT; responsible for digital electronics and EGSE.

"COS-B Experiment for Gamma Ray Astronomy", Space Sci. Instr. 1, 245 (1975).

"Preliminary Results from COS-B", NASA CP002 (1976).

K. Bennett, Staff Scientist; gamma ray astronomy; balloon payloads; COS-B; Experiment Manager.

"A Drift Chamber Detector for Gamma Ray Astronomy", Nucl. Instr. Meth. (1977).

"COS-B Observations of Galactic Gamma Ray Emission", ESA SP 124, 83 (1977).

D. Wills, Staff Scientist; gamma ray astronomy; OGO-5 and COS-B (Project Scientist and Co-Investigator); Experiment Scientist.

"COS-B Experiment for Gamma Ray Astronomy", Space Sci. Instr. 1, 245 (1975).

"COS-B Observations of Localised Emission in the Anti-Centre", Astron. Astrophys. 56, 461 (1977).

7. Conclusions

Gamma ray astronomy in the 1-30 MeV energy range is fully open for investigation provided a low instrumental background is combined with good angular and energy resolution in one instrument. The proposed experiment fulfills this requirement to the maximum extent possible within the available technology. All critical aspects of the concept and the design are proven by balloon programmes. This experiment has the potential to provide a breakthrough in medium energy gamma ray astronomy comparable to that made by UHURU in X-ray astronomy.

Appendix A.1

Sensitivity calculation

The formulae used for the calculation of minimum source detectability and source location accuracy for an Imaging Compton Telescope are derived using the following parameters:

- m confidence level (σ)
- A effective sensitive area (cm^2)
- T effective observation time (s)
- N counts due to source and background
- $\Delta\omega$ effective resolution elements (sr)
- φ Compton scatter angle (rad)
- σ_φ 1-σ angular resolution (rad)
- I_c cosmic background intensity ($cm^{-2}s^{-1}sr^{-1}$)
- I_b instrumental background converted to the corresponding cosmic background intensity ($cm^{-2}s^{-1}sr^{-1}$)
- I_s source intensity ($cm^{-1}s^{-1}$)
- I_i intensity of other source (i) in field of view ($cm^{-2}s^{-1}$)
- f_i fraction of counts from source i contributing to background

The formulae can be applied to any energy interval, provided the parameters are correctly averaged over the interval.

The minimum source detectability in the case of simultaneous source and background observation is given by

$$I_s = \frac{m}{A\,T}\sqrt{N} \qquad (1)$$

in which N includes background and source counts. For any imaging detector only background in a well defined resolution element $\Delta\omega$ need be considered. In the case of the Compton telescope we have

$$N = A\,T\,[I_c(1+\delta) + I_b]\,\Delta\omega + A\,T\,[I_s + (1+\delta)\sum_i f_i\,I_i] \qquad (2)$$

The factor $(1+\delta)$ accounts for the partially absorbed events. These events are not accepted from the source, but contribute to the background. The value of δ ranges from 0.15 at 1 MeV to 0.45 at 30 MeV. The term $\sum_i f_i I_i$ reflects the background resulting from possible nearby sources ($0 \le f_i \le 1$, see below).

Referring back to Figure 8 (section 2.1) it is easily understood that

$$\Delta\omega(\varphi) = 2\,\pi \sin\varphi \cdot \Delta\varphi \qquad (3)$$

where $\Delta\varphi$ represents the effective width of the events circles. The appropriate value for $\Delta\varphi$ is

$$\Delta\varphi = 3.5\,\sigma_\varphi = 1.5 \cdot \mathrm{FWHM} \qquad (4)$$

as determined from the image reconstruction in the presence of background using cross-correlation methods. After averaging $\Delta\omega$ over all accepted values of φ (within the event selection criteria), taking the Compton scatter probability as a function of φ into account, we may write

$$\langle \Delta\omega \rangle = 7\ \pi \sin \varphi' \cdot \sigma_{\varphi} \qquad (5)$$

where φ' is the effective scatter angle. The values for σ_{φ} in eq. 5 are given in Figure 15. The values for $\Delta\omega$, derived for the standard selection criteria, are given in Figure A.1.

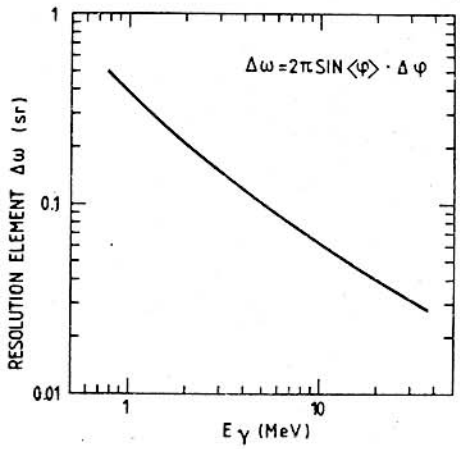

Fig. A.1: Effective resolution element (eq. 5).

A fraction f_i of gamma rays from any other source in the field of view cannot be distringuished from the real source counts. For totally unresolved sources $f_i = 1$. However, f_i drops rapidly to values ≤ 0.1 at separations $\geq 5\ \sigma_{\varphi}$. Therefore in most practical cases the contribution of $\Sigma f_i I_i$ to the outcome of eq. 2 is negligible. This fact is illustrated in Figure 16, which clearly indicates that sources of comparable intensity will still be resolved if their separation is 2-3 σ_{φ}. Therefore

$$I_s = m \sqrt{\frac{[I_c(1+\delta) + I_b]\ \langle \Delta\omega \rangle + I_s}{AT}} \qquad (6)$$

Points on the event circles nearest the true source position obey a two-dimensional gaussian distribution defined by $\sigma = \sigma_{\varphi}$. The 90% confidence error radius for the derived source position is then

$$r = \frac{2.15}{m}\ \sigma_{\varphi} \qquad (7)$$

For the detectability of extended one-dimensional sources (e.g. galactic plane) of length Δl one substitutes in eq. 6

$$\langle \Delta\omega \rangle \simeq 7\ \pi \sin \varphi'\ \sigma_{\varphi}\ (1 + \frac{2\ \Delta l}{\pi \varphi'}) \qquad (8)$$

Linear polarization of gamma rays from a point source will produce a deviation from rotational symmetry of the scattered gamma ray directions (S' in Figure 8). The magnitude depends on energy and scatter angle (Figure 19). Using these data, averaged within the standard event selection criteria, gives a value of 5% for the detection efficiency of polarization in the energy range 1-5 MeV. Polarized radiation may thus be detected at a level

$$I_p = \frac{m}{0.05} \sqrt{\frac{[I_c(1+\delta) + I_b]\ \langle \Delta\omega \rangle + I_s}{AT}} \qquad (9)$$

The average exposure $\langle AT \rangle$ for any point in the sky obtained with approximately uniform exposure over a sky element ω' in a time period T', is given by

$$\langle AT \rangle = \frac{A\ \omega T'}{\omega'}$$

where $A\omega$ is the effective geometrical factor (Figure 18). A full sky coverage in two years will result in detection limits at any point in the sky similar to those obtained after a 1 month pointing.

Appendix A.2

References

Albats, P., Frye, G.M.,Jr., Mace, O.B., Hopper, V.D., Thomas, J.A.: 1972, Nature 240, 221.

Baity, W.A., Jones, T.W., Wheaton, W.M.A. and Peterson, L.E.: 1975, Ap. J. 199, L5.

Baker, R.E., Lovett, R.R., Orford, K.J., Ramsden, D.: 1973, Nature Phys. Sc. 245, 18.

Bennett, K., Bignami, G.F., Boella, G., Buccheri, R., Hermsen, W., Kanbach, G., Lichti, G.G., Masnou, J.L., Mayer-Hasselwander, H.A., Paul, J.A., Scarsi, L., Swanenburg, B.N., Taylor, B.G. and Wills, R.D.: 1977, Astron. Astrophys. 61, 279.

Bleeker, J.A.M. and Deerenberg, A.J.M.,:1970, Ap.J. 159, 215.

Chupp, E.L., Forrest, D.J., Higbie, P.R., Suri, A.N., Tsai, C. and Dunphy, P.P.: 1973, Nature 241, 333.

Clayton, D.D.: 1971, Nature 234, 291.

Clayton, D.D., Colgate, S.A. and Fishman, G.J.: 1969, Ap. J. 155, 75.

Daniel, R.R. and Lavakare, P.J.: 1975, Pramana, Vol. 5, No. 3, 107.

Daugherty, J. and Schönfelder, V.: 1977, Space Sci. Instr. 3, No. 4.

Fichtel, C.E., Hartman, R.C., Kniffen, D.A., Thompson, D.J., Bignami, G.F., Ögelman, H., Özel, M.E. and Tümer, T.: 1975, Ap. J. 198, 163.

Fichtel, C.E., Hartman, R.C., Kniffen, D.A., Thompson, D.J., Ögelman, H.B., Özel, M.E., Tümer, T.: 1977, Proc. 12th ESLAB-Symp. "Recent Advances in Gamma Ray Astronomy", ESA SP 124, 191.

Fishman, G.J., Harnden, F.R., and Haymes, R.C.:1970, in L. Gratton (ed.), Non-Solar X- and Gamma Ray Astronomy, IAU Symp. 37, 116.

Fishman, G.J., Harnden, F.R.,Jr., Johnson III, W.N., Haymes, R.C.: 1969, Ap. J., 158, L61.

Fukuda, Y., Hayakawa, S., Kasahara, I., Makino, F., Tanaka, Y. and Screekantan, B.V.: 1975, Nature 254, 398.

Gruber, D.E. and Ling, J.C.: 1977, Ap. J. 213, 802.

Gumplinger, P.: 1978, ingeneer thesis at the MPI, to be published.

Hall, R.D., Meegan, C.A., Walraven, G.D., Djuth, F.T. and Haymes, R.C.: 1976, Ap. J. 210, 631.

Haymes, R.C., Harnden, F.R.,Jr., Johnson III, W.N. and Prichard, H.M.: 1972, Ap. J. 172, L47.

Haymes, R.C., Walraven, G.D., Meegan, C.A., Hall, R.D., Djuth, F.T. and Shelton, D.H.: 1975, Ap. J. 201, 593.

Helmken, H.F. and Hoffman, J.A.: 1973, Nature Phys. Sci 243, 6.

Hermsen, W., Bennett, K., Bignami, G.F., Boella, G., Buccheri, R., Higdon, J.C., Kanbach, G., Lichti, G.G., Masnou, J.L., Mayer-Hasselwander, H.A., Paul, J.A., Scarsi, L., Swanenburg, B.N., Taylor, B.G. and Wills, R.D.: 1977, Nature 269, 494.

Jacobson, A.S.: 1977, Invited paper Spring Meeting A.P.S., Washington, April 1977.

Kraushaar, W.L., Clark, G.W., Garmire, G.P., Borken, R., Higbie, P., Leong, C., Thorsos, T.: 1972, Ap. J. 177, 341.

Kuo Fu-Shong, Fry, G.M. and Zych, A.D.: 1973, Ap. J. 186, L51.

Kurfess, J.D.: 1971, Ap. J. 168, L39.

Lampton, M., Margon, B., Bowyer, S., Mahoney, W. and Anderson, K.: 1972, Ap. J. 171, L45.

Laros, J.G., Matteson, J.L., Pelling, R.M.: 1973, Nature Phys. Sci. 246, 109.

Lingenfelter, R.E. and Ramaty, R.: 1976, Symp. on the Structure and Content of the Galaxy and Galactic Gamma Rays, eds. C.E. Fichtel and F. Stecker, NASA CP-002, 237.

Lingenfelter, R.E. and Ramaty, R.: 1977, Ap. J. 211, L19.

Mazets, E.P., Golenetskii, S.V. and Ilinskii, V.N.: 1977, Ap. J. Lett. 18, 155.

Mazets, E.P., Golenetskii, S.V., Ilinskii, V.N., Guvyan, Yu. A. and Kharitonova, T.V.: 1974, Joffe Physico Technical Institute, preprint no. 468.

Mushotzky, R.F., Baity, W.A., Wheaton, W.A. and Peterson, L.E.: 1975. 146th Am. Astron. Soc. Meeting, San Diego, August 1975.

Mushotzky, R.F., Baity, W.A., Wheaton, W.A. and Peterson, L.E.: 1976, Ap. J. 206, L45.

Mitchell, E.: 1977, Internal report at the MPI.

Paciesas, W.S., Mushotzky, R.F. and Pelling, R.M.: 1976, in Ph.D. thesis Mushotzky, Univ. of Calif., San Diego.

Parlier, B., Forichon, M., Montmerle, T., Agrinier, B., Boella, G., Scarsi, L., Niel, M. and Palmeira, R.: 1975, Proc. 14th Intern. Cosmic Ray Conf., München, 1, 14.

Paul, J.A., Bennett, K., Bignami, G.F., Buccheri, R., Caraveo, P., Hermsen, W., Kanbach, G., Mayer-Hasselwander, H.A., Scarsi, L., Swanenburg, B.N., Wills, R.D.: 1978, accepted by Astron. Astrophys.

Peterson, L.E.: 1967, Ann. Rev. Astron. Astroph. 13, 473.

Peterson, L.E.: 1965: J.G.R. 70, 1762.

Ramaty, R., Börner, G., Cohen, J.M.: 1973, Ap. J. 181, 891.

Ramaty, R., Kozlovski, B. and Lingenfelter, R.E.: 1975, Space Sci. Rev., 18, 341.

Schönfelder, V.: 1977, 15th Intern. Cosmic Ray Conf., Plovdiv, Vol. 10.

Schönfelder, V., Graser, U. and Daugherty, J.: 1977, Ap. J. 217, 306.

Schönfelder, V., Lichti, G. and Moyano, C.: 1975, Nature 257, 375.

Share, G.H., Kinzer, R.L., Samini, J. and Jabbari-Azad, J.: 1977, Proc. 12th ESLAB-Symp. "Recent Advances in Gamma Ray Astronomy", ESA SP 124, 107.

Thompson, D.J., Fichtel, C.E., Hartman, R.C., Kniffen, D.A., Lamb, R.C.: 1977, Ap. J. 213, 252.

Trombka, J.I., Dyer, C.S., Evans, L.G., Bielefeld, M.J., Seltzer, S.M. and Metzger, A.E.: 1977, Ap. J. 212, 925.

Vedrenne, G., Alberne, F., Martin, I., Talon, R.: 1971, Astron. Astroph. 15, 50.

Walraven, G.D., Hall, R.D., Meegan, C.A., Coleman, P.L., Shelton, D.H., Haymes, R.C.: 1975, Ap. J. 202, 502.

White, R.S., Dayton, B., Moon, S.H. Ryan, J.M., Wilson, R.B. and Zych, A.D.: 1977, preprint no. IGPP-UCR-77-6, Univ. of California, Riverside.

Wilson, R.B., Moon, S., Ryan, J., Zych, A.D., White, R.S. and Dayton, B.: 1977, Proc. 15th Intern. Cosmic Ray Conf., Plovdiv, Vol. 1, 24.

Young, P.G. and Forster, D.G., Jr.: 1972, Los Alamos Rep., LA-4726.

ARBEITSAUFTEILUNG COMPTEL

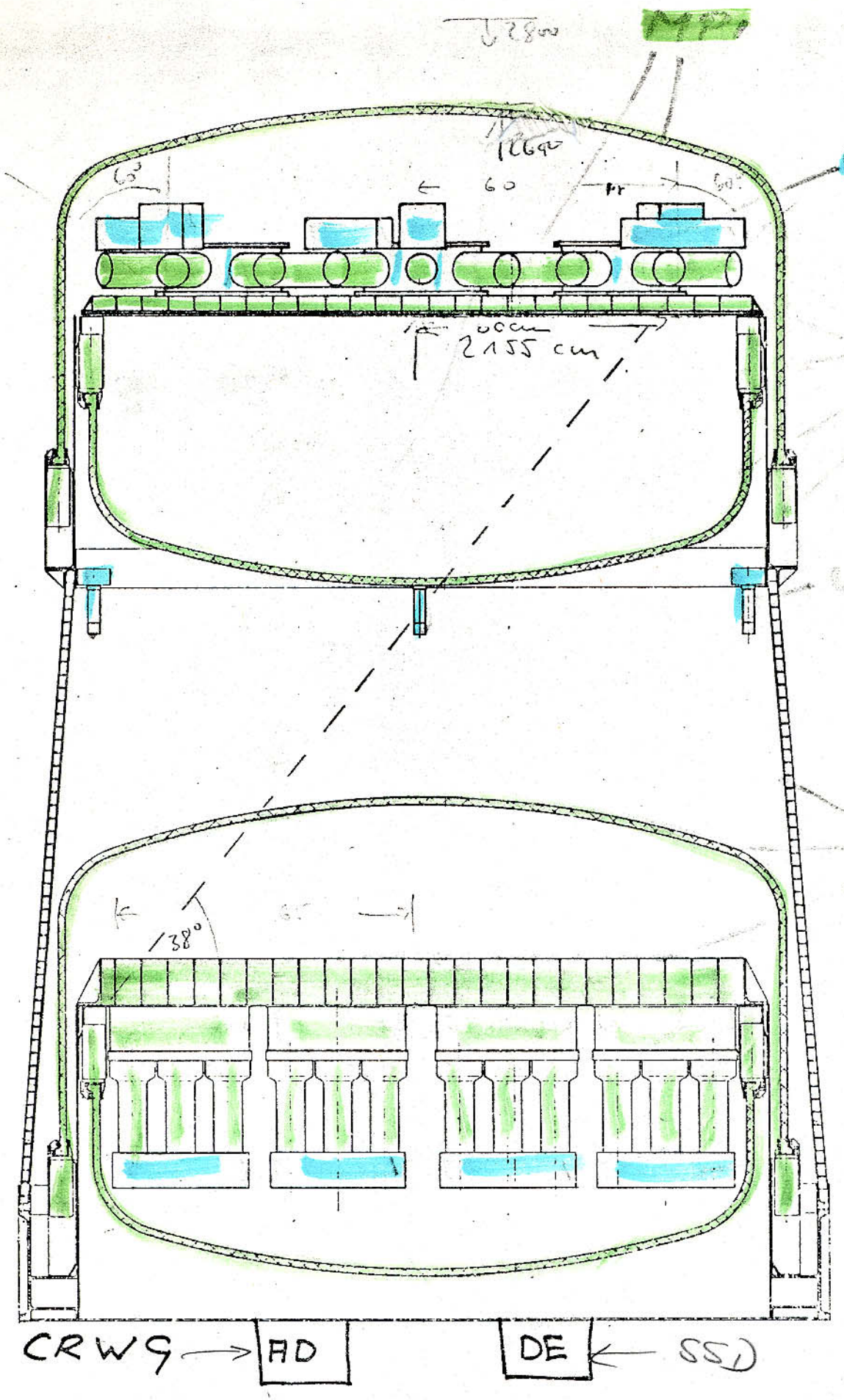

UNH: University of New Hampshire
CRWG: Cosmic Ray Working Group
SSD: Space Science Department of ESA

AE: Analogelektronik
DE: Digitalelektronik